To appear in the Proceedings of the XI Canary Islands Winter School Of Astrophysics on "Galaxies at High Redshift", Tenerife November 1999, I. Perez-Fournon, M. Balcells, F. Moreno-Insertis and F. Sanchez Eds., Cambridge University Press;
astro-ph/0009121

High-Redshift Galaxies: The Far-Infrared and Sub-Millimeter View

Alberto Franceschini

Dipartimento di Astronomia, University of Padova, I-35122 Padova, IT

Abstract. Observations at long wavelengths, in the wide interval from a few to 1000 μm, are essential to study diffuse media in galaxies, including all kinds of atomic, ionic and molecular gases and dust grains. Hence they are particularly suited to investigate the early phases in galaxy evolution, when a very rich ISM is present in the forming systems.

During the last few years a variety of observational campaigns in the far-IR/sub-mm, exploiting both ground-based and space instrumentation, have started to provide results of relevant cosmological impact. Most crucial among these have been the discovery of an intense diffuse background in the far-IR/sub-mm of extragalactic origin, and the deep explorations from space in the far-IR and with large millimetric telescopes on ground. These results challenge those obtained from optical-UV observations, by revealing luminous to very luminous phases in galaxy evolution at substantial redshifts, likely corresponding to violent events of star-formation in massive systems. This is bringing to significant refinements of the present schemes of galaxy formation, as far as the history of baryon transformations is concerned.

Table of Contents

- INTRODUCTION
  - The history of baryon transformations
  - Long-wavelength observations of galaxies: a view on the diffuse media and on the "active" phases in galaxy evolution
  - Observational issues
  - These lectures
- DUST IN GALAXIES
  - Generalities
  - Dust grains in the ISM
    - Grain production
    - Grain destruction
    - The evolution of the dust content in a galaxy
  - Interactions between dust and radiation
  - Alternative heating mechanisms for dust
  - The interstellar extinction curve
  - Models of the interstellar dust
- EVALUATING THE DUST EMISSION SPECTRA
  - Radiative transfer in thick dusty media
    - Numerical solutions based on iterative schemes
    - Monte Carlo solutions
- GENERALIZED SPECTRO-PHOTOMETRIC MODELS OF GALAXIES
  - Semi-empirical approaches
  - Detailed self-consistent spectro-photometric models
    - Chemical evolution of the ISM
    - Geometrical distributions of gas and stars
    - Models of the molecular clouds (MC)
    - Models of diffuse dust (cirrus)

- Modelling the SEDs of normal and starburst galaxies

- INFRARED AND SUB-MM LINE SPECTRA
  - The cold molecular gas
  - The cold neutral gas
  - The ionized component of the ISM

- IR STARBURST AND ULTRA-LUMINOUS GALAXIES IN THE LOCAL UNIVERSE
  - The infrared-radio correlation
  - Estimates of the star formation rate (SFR)
  - Gas reservoirs, depletion times, starburst duration
  - Starburst-driven super-winds
  - Starburst models
  - Statistical properties of active galaxy populations
  - Starburst triggering
  - Ultra-luminous IR galaxies (ULIRGs)
  - Origin of elliptical galaxies and galaxy spheroids

- IR GALAXIES IN THE DISTANT UNIVERSE: PRE-ISO/SCUBA RESULTS

- THE BREAKTHROUGHS: DISCOVERY OF THE CIRB
  - Observational status about the CIRB
  - Constraints from observations of the cosmic high-energy opacity
  - Contribution of cosmic sources to the CIRB: the formalism
    - Source contribution to the background intensity
    - Small scale intensity fluctuations

- DEEP SKY SURVEYS WITH THE INFRARED SPACE OBSERVATORY (ISO)
  - Motivations for deep ISO surveys
  - Overview of the main ISO surveys
    - The ISOCAM Guaranteed Time (GT) Extragalactic Surveys
    - The European Large Area ISO Survey (ELAIS)
    - The ISOCAM observations of the two Hubble Deep Fields
    - ISOCAM survey of two CFRS fields
    - The ISOPHOT FIRBACK survey program
    - The Lensing Cluster Surveys
    - The Japanese Guaranteed Time surveys
  - Data reduction
  - Mid-IR and far-IR source counts from ISO surveys

- EXPLORATIONS OF THE DEEP UNIVERSE BY LARGE MILLIMETRIC TELESCOPES

- INTERPRETATIONS OF FAINT IR/MM GALAXY COUNTS
  - Predictions for non-evolving source populations in the mid-IR
  - Evidence for a strongly evolving population of mid-IR galaxies
  - A panchromatic view of IR galaxy evolution

- NATURE OF THE FAST EVOLVING SOURCE POPULATION
  - Tests of the evolving IR population in the HDFs and CFRS fields
    - Optical and NIR spectral properties: nature of the IR sources
    - Evaluating baryonic masses and the SFR of the IR population
  - What are the FIRBACK 175 μm sources?
  - The nature of the high-z galaxies detected in the millimeter
  - AGN contribution to the energetics of the faint IR sources
  - Discussion

- GLOBAL PROPERTIES: THE SFR DENSITY AND CONTRIBUTIONS TO THE CIRB
  - Evolution of the comoving luminosity density and SFR
  - Energy constraints from background observations
    - Constraints from the integrated optical background
    - Explaining the CIRB background

- Galactic winds and metal pollution of the inter-cluster medium
- A two-phase star-formation: origin of galactic disks and spheroids
- Contribution by gravitational accretion to the global energetics

- CONCLUSIONS

- REFERENCES

1. INTRODUCTION

1.1. The history of baryon transformations

Although baryons contribute a negligible fraction of the global mass density of the universe, their transformations and the associated energy releases are key elements of the complex, puzzling history bringing from the primeval undifferentiated plasma to the highly structured present-day universe.

Two main driving mechanisms are able to circulate and transform baryons in astrophysical systems: one is related with stars and thermonuclear processes occurring therein, the other with gravitational contraction of gas - an important aspect of which, able to generate vast amounts of energy and producing spectacular effects in Active Galactic Nuclei and quasars, is gravitational accretion onto supermassive black holes.

Obviously, these two fundamental motors of the baryon cycle produce very different outcomes. While gravitational BH accretion irreversibly destroys baryons to produce energy, gas cycling into stars has (more beneficial) effects originating beautiful stellar systems, producing soft-energy photons, heavy elements, dust, and planetary systems in the proper amounts to bring eventually to the life.

A basic aim of the present studies of the distant universe, exploiting the current most powerful astronomical instrumentation, is indeed to clarify the history of baryon circulation, and in particular the paths through which the various different galaxy populations, which we observe in the local universe, have built their stellar content, created their hosted nuclear BH's and accumulated material in them.

While the overall story is driven by the evolving background of dark matter distribution, baryons are the observable traces of the evolving large scale structure.

The history of star formation, in particular, is a fundamental descriptor of cosmic evolution. Different cosmogonic scenarios predict very different timetables for the formation of stars and structures. For example, some models predict substantially different formation epochs for stars among the various morphological classes of galaxies, in particular between early-type and late-type galaxy systems. Some others, notably some specializations of the Cold Dark Matter-dominated models, do not.

1.2. Long-wavelength observations of galaxies: a view on the diffuse media and on the "active" phases in galaxy evolution

The build up of stellar populations in high-redshift galaxies is most usually investigated by looking at the optical/UV/near-IR emission from already formed stars in distant galaxies. The complementary approach, less frequently used, is to look at the diffuse media - atomic and molecular gas and dust - in high-z systems, and their progressive transformation into stars.

While observations of the redshifted starlight emission in the optical/near-IR can exploit large telescopes on ground and very efficient photon detectors, reliable probes of the diffuse media require longer-wavelength observations in the far-IR and sub-millimeter: a large variety of lines from atomic species and molecules in the Inter-Stellar Medium (ISM) at all ionization levels are observable there. Another fundamental component of the ISM, dust grains present in all astrophysical settings ranging from planetary disks to nuclear accretion torii around quasars, have the property to emit at these wavelengths, typically between a few μm to 1000 μm.

Observations at long- λ are then essential to study diffuse media in galaxies and *are particularly suited [and needed] to study the early phases in galaxy evolution, when a very rich ISM is present in the forming system*.

Under the generic definition of *galaxy activity* we indicate transient phases in the secular evolution of a galaxy during which the various transformations of the baryons undergo a significant enhancement with respect to the average rate, for reasons to be ascertained. These phenomena concern both enhanced rates of conversion of the ISM gas into stars (the *starburst* phenomenon), and phases of increased activity of the nuclear emission following an event of fast accretion of gas into the super-massive BH (the so-called AGN phase, reaching parossistic levels of photon production of up to $\sim 10^{50} erg/s$ in some high-z quasars).

As we will describe in this paper, IR and sub-mm wavelengths provide a privileged viewpoint to investigate galaxy "activity" in general, for two main reasons: (a) in many cases this λ-interval includes a dominant fraction of the whole bolometric output of active objects; (b) at long wavelengths the screening effect of diffuse dust, present in large amounts in "active" galaxies, is no more effective and an impeded access to even the most extreme column-density regions is possible.

1.3. Observational issues

Unfortunately, the IR and sub-millimeter constitute a very difficult domain to access for astronomy: from ground this is possible only in a few narrow bands from 2.5 to 30 μm and at λ > 300 μm. From 30 to 300 μm observations are only possible from space platforms, the atmosphere being completely opaque.

In any case, however, infrared observations even from space are seriously limited by several factors. The most fundamental limitation is intrinsic in the energies ϵ of photons we are looking at: the quantum-mechanics uncertainty principle sets a boundary to the best achievable angular resolution θ due to diffraction of photons in the primary mirror of a telescope of size D: $\theta[FWHM] \geq 1.4*57.3*3600\ \lambda/D$ [*arcsec*], ($\lambda = ch/\epsilon$). For a typical cooled space telescope of 1 meter diameter working at λ = 100 μm this corresponds to $\theta \sim 30$ *arcsec*. For deep surveys of high-redshift IR galaxies this limited spatial resolution implies a limiting flux detectable above the noise due to confusion of several faint sources in the same elementary sky pixel. This confusion limit sets in at flux levels corresponding to $\sim 0.04\ sources/area\ element$, or 0.16 sources/$arcmin^2$ = 570 $sources/degree^2$ in the above example (see eq. [8.26] and further details below). On this regard, recent surveys (see Sects. 10 and 11) have revealed that the far-IR sky is very much populated by luminous extragalactic sources, which implies that confusion starts to manifest already at relatively bright fluxes for even large space observatories.

Other limiting factors for IR observations come from the difficulty to reduce the instrumental background of (even space) telescopes due to photons generated by the optics. This adds to the ambient photon backgrounds, due to Zodiacal light from interplanetary dust, dust emission from the Milky Way, and the terrestrial atmospheric emission.

The instrumental backgrounds are reduced by cooling the instrumentation, in particular for space IR observatories, but this requires either inserting the whole telescope in large dewars (ISO, SIRTF), or by passively cooling the telescope with a very efficient Sun-shielding (FIRST, NGST). All this is technologically very much demanding and tends to limit the duration of space IR missions (because of the finite reservoir of coolant) and the size of the primary photon collector.

Finally, photon detection is not as easy in the IR as it is in the optical, and limited performances are offered by bolometers in the sub-mm and by photo-conductors in the mid- and far-IR. Furthermore, the need to cool detectors to fundamental temperatures entails problems of response hysteresis and detector instabilities due to slow reaction of the electrons to the incoming signal.

1.4. These lectures

In spite of the mentioned difficulties to observe at long wavelengths, it was clear since the IRAS survey in 1984 that very important phenomena can be investigated here. Only recently, however, pioneering explorations of the high-redshift universe at these long-wavelengths have been made possible by new space and ground-based facilities, and a new important chapter of observational cosmology has been opened.

These lectures are dedicated to a preliminary assessment of some results in the field. Because of the very complex, often still elusive, nature of many of the discovered sources, and because of the complicated astrophysical processes involved, we dedicate a significant fraction of this paper to review properties of diffuse media (particularly dust) in local galaxies, and of their relation with stars (Sects. 2, 3, 4 and 5). We also devote a substantial chapter (Sect. 6) to the description of local IR starbursts and ultra-luminous IR galaxies, to improve our chances of understanding their high-redshift counterparts.

Then after a brief mention of historical (IRAS) results in the field (Sect. 7), we come to discuss in Sect. 8 the discovery and recent findings about the Cosmic Infrared Background (CIRB), in Sect. 9 the deep IR surveys by the Infrared Space Observatory (ISO), and in Sect. 10 the pioneering observations by millimetric telescopes (SCUBA, IRAM). Interpretations of the deep counts are given in Sect. 11, and the question of the nature of the fast-evolving IR source populations is addressed in Sect. 12. Sect. 13 is dedicated to discuss the global properties of the population and some constraints set by the CIRB observations. A concise summary is given in Sect. 14. A Hubble constant H_0 = 50 *Km/s/Mpc* will be adopted unless otherwise stated.

2. DUST IN GALAXIES

2.1. Generalities

Dust is one of the most important components of the ISM, including roughly half of heavy elements synthesized by stars. The presence of dust is relevant in many astrophysical environments and has a crucial role in shaping the spectra of many cosmic bodies. However, its existence has been inferred from very indirect evidences up untill recently. The first evidence came from the discovery of a tenuous screen of small particles around the Earth producing the *zodiacal light*. Other evidences came from observations of dust trails of comets, circumstellar dust envelopes around evolved stars, diffuse dust in the MW producing the interstellar extinction, the discovery of IR emission by galaxies and ultra-luminous IR galaxies in the IRAS era, circumnuclear dust in AGNs (essential ingredient of the unified model for AGNs), the cosmological IR background (COBE, 1996-1998), and eventually the discovery of sites of extremely active star formation at high redshifts (SCUBA and ISO, 1998-2000).

Accounting for the effects of dust is essential not only to understand the erosion of optical light, but, even more importantly, to evaluate the energy re-emitted by dust at longer wavelengths, typically at $\lambda \sim 5$ to 1000 μ. This is crucial for estimating all basic properties of distant galaxies: the *Star Formation Rate* (SFR) from various optical and IR indicators, the *ages of stellar populations*, which, based as they are on optical colours, have to distinguish the reddening of the spectrum due to aging from that due to dust extinction, and finally to constrain the stellar *initial mass function* (IMF).

2.2. Dust grains in the ISM

Rather than by stars, the available volume in a galaxy is occupied by the ISM, which in local late-type systems amounts to $\sim$ 10% of the baryonic mass. The ISM includes gas mixed with tiny solid particles, the *dust*, with sizes ranging from a few Å (the PAH molecules) up to $\sim 10\,\mu$m. The mass in dust is typically 0.5 to 1% of the ISM mass.

2.2.1. *Grain production*

The mechanisms of birth, growth and destruction of grains are very complex and poorly understood. It is believed that condensation nuclei for dust grains mostly form in dense regions of the ISM, which are better shielded from UV photons. Main dust production sites are hereby listed.

Envelopes of protostars: during the process leading to the birth of a star a solar nebula is produced, where silicate grains can be formed and then blown away by a Pre-Main Sequence wind (T Tauri phase).

Cold evolved stars: in the cold atmospheres of evolved giants, dust grains can form and drive a strong stellar wind, in particular graphite grains from carbon stars and silicate grains in OH-IR stars. Stars with $M < 8 M_{\odot}$ are important dust producers;

higher-*M* stars, like Wolf-Rayets with high mass-loss rates, are too rare.

Type-II supernovae are probably the most important contributors, as revealed by a variety of tests, like those provided by the IR excesses in the light-curve and the extinction of background stars in SN ejecta. Direct evidences of dust production came from the case-study of SN 1987a (CO and SiO molecules found in the ejecta), the dark spots observed in the synchrotron nebula of Crab, the IR mapping by ISO of Cas-A which resolved clumpy emission associated with the fast moving knots (Lagage et al. 1996).

Type-I supernovae have an uncertain role, with no evidence yet for dust formation (which would be otherwise relevant to solve the problem of the Fe depletion).

The general interstellar medium is also the site of a slow growth around pre-existent condensation nuclei (refractory cores); it is in this way that dirty icy grains are produced.

2.2.2. *Grain destruction*

Grain survival is another, uncertain, chapter of the complex story of dust enrichment of the ISM. Grain destruction is not likely a problem in stellar winds, the grain should survive the injection into the ISM, while it is more a problem for SN ejecta (which have typical velocities in excess of 1000 *Km/s*).

Even after the ejection phase, the ISM is in any case a difficult environment for grain survival: grains can be destroyed there by evaporation, thermal sublimation in intense radiation fields, evaporation in grain-grain collisions, and by radiative SN shocks.

2.2.3. *The evolution of the dust content in a galaxy*

Modelling the complex balance between grain production and destruction is also guided by observations of isotopic anomalies

in meteorites and of the elemental depletion pattern. A detailed account of most plausible intervening processes in the dust life cycle can be found in Dwek (1998). The author also discusses evolution paths of the elemental abundances in the gas and dust phases in a typical spiral galaxy, based on standard assumptions for the infall of primordial gas and chemical evolution. Type-II SN are found to be the main producers of silicate dust in a galaxy, while carbon dust is due to lower mass (2-5 $M_\odot$) stars. The different lifetimes of the two imply likely anomalous abundance ratios between the various dust grain types during the course of galaxy evolution, naturally evolving from an excess of silicate to an excess of carbon grains with galactic time.

Altogether, the dust mass is found to be linearly proportional to the gas metallicity and equal to 40% of the total mass in heavy elements in a present-day galaxy. Although the details can depend to some extent on the evolution of the SFR with time (e.g. in the case of elliptical galaxies this evolution could have been more rapid, see Mazzei, De Zotti & Xu 1994), these general results are not believed to be much affected.

2.3. Interactions between dust and radiation

Dust particles interact with photons emitted by astrophysical sources by absorbing, scattering, and polarizing the light (the combined effect of absorption and scattering takes the name of *extinction*). They also emit photons at wavelengths typically much greater than those of the absorbed photons. The total intensity radiation field $I_\nu(\vec{r}, t)$ (defined as usual by $dE \equiv I_\nu d\nu d\Omega dA dt$, dE being the differential amount of radiant energy) is related to the field sources by the *transfer equation*:

$$\frac{dI_\nu}{d\tau} = -I_\nu + S_\nu, \quad (2.1)$$

where $d\tau_\nu \equiv \alpha_\nu ds$ is the differential optical depth corresponding to a spatial path ds, $S_\nu \equiv j_\nu / \alpha_\nu$ is the *source function*, α_ν and j_ν being the *extinction* (true absorption + scattering) and emission (true emission + scattering) coefficients. A medium is said *optically thin* or *thick* if τ_ν along a typical path trough the medium is << 1 or >> 1. Absorption includes those processes in which the energy of photons is turned into other forms (may be internal energy of matter or fields), true emission is the opposite processe, whilst in scattering the energy of photons is simply *deviated* into other directions. Dust scattering is usually elastic. A formal solution to eq.(1) [e.g. Rybicki & Lightman 1979] is given by:

$$I_\nu(\tau_\nu) = I_\nu(0)\exp(-\tau_\nu) + \int_0^{\tau_\nu} \exp(-\tau_\nu + \tau'_\nu)\, S_\nu(\tau'_\nu)\, d\tau'_\nu \quad (2.2)$$

If each dust grain has a λ-dependent effective *cross section* σ_ν and spatial density n, then $\alpha_\nu = n\ \sigma_\nu$ or $\tau_\nu = N\ \sigma_\nu$, where N is the *column density*. For dust grains it is common to write

$$\sigma_\nu = Q_{\nu,e}\,\sigma_g = (Q_{\nu,a} + Q_{\nu,s})\,\sigma_g$$

where σ_g is the geometrical cross section (πa^2 for spheres) and $Q_{\nu,e}$ is the extinction efficiency (true absorption scattering). At short- λ (UV), diffraction effects in the photon-grain interaction become negligible, and the effectiv cross-section coincides with the geometric one, $Q_{\nu,e} \sim 1$. Altogether: $\alpha_\nu = Q_{\nu,e}\,\sigma_g\ n$.

The albedo $a_\nu = Q_{\nu,s}/Q_{\nu,e}$ is the fraction of extinguished light being scattered by the grain rather than absorbed.

The emission coefficient j_ν includes a *true* emission $j_{\nu,e}$ and an elastic scattering component, $j_{\nu,s}$, given by:

$$j_{\nu,s}(\hat{\omega}) = Q_{\nu,s}\sigma_g\, n_d\, \frac{1}{4\pi}\int_{4\pi} I_\nu(\hat{\omega}')f_\nu(\hat{\omega} - \hat{\omega}')d\Omega$$

where f_ν is the *phase function*, depending on the incidence-scattering angle.

The true emission of dust grains is thermal. From Kirchoff's law [$j_\nu = \alpha_\nu B_\nu(T)$]:

$$j_{\nu,e} = n_d Q_{\nu,a} \sigma_g B_\nu(T_d). \quad (2.3)$$

It is clear that both terms of the emission coefficient depend on the radiation field I_ν. In particular $j_{\nu,e}$ depends on it trough the dust grain temperature T: grain heating is almost always dominated by the radiation field. Thus a primary task is to compute T. Two situations apply.

(a) Grains sufficiently large and massive don't cool in the time interval between absorption of two photons: they are in thermal equilibrium with the radiation field. Their temperature can be determined by solving for T an energy conservation equation *absorbed energy = emitted energy*:

$$\int Q_{\nu,a} J_\nu \, d\nu = \int Q_{\nu,a} B_\nu(T) \, d\nu \quad (2.4)$$

where $J_\nu = 1/4\,\pi \int I(\nu, \omega) d\Omega$ is the angle-averaged I_ν.

(b) Small grains fluctuate in temperature at any acquired photon. They never reach thermodynamic equilibrium (the cooling time is shorter than that between two photons arrivals). A probability distribution $P(T)dT$ to find a grain between T and $T + dT$ can then be computed based on a statistical approach (Puget et al. 1985; Guhathakurta & Draine 1989, Siebenmorgen & Kruegel 1992). Basic ingredients for this computation are:

- the specific heat $C(T, a)$ per C-atom of PAH's of size a and the number N_c of C atoms in the grain;

- the maximum T a PAH can attain after absorption of a photon $h\nu$, and given by the relation:

$$h\nu' = \int_{T_{min}}^{T_{max}} N_c(\nu', a) C(T, a) dT;$$

- the cooling rate of a PAH after being heated to T_{max} is

$$dT/dt = \frac{4\pi a^2 F(T, a)}{C(T, a)}$$

where $F(T, a) = \int Q_{abs}(\nu, a)\, \pi B(\nu, T) d\nu$ is the power radiated per unit grain surface. The total IR spectrum radiated during the cooling down is:

$$S(\nu', \nu, a) = \int_0^t dt\ \pi B(\nu, T) Q_a(\nu, a) 4\pi a^2 = \int_{T_{min}}^{T_{max}} dT\ \pi B(\nu, T) Q_a(\nu, a) \frac{N_c\, C(T, a)}{F(T, a)}.$$

In any case, dust grains are destroyed by radiation-induced temperatures above $\sim$ 1000 ÷ 2000 K (depending mainly on composition). This is the reason why their emission is relevant only longwards a few μm.

For mixtures of different species of particles the equations must be summed over all the species. For spherical grains of different compositions and sizes a and density $n_i(a)$:

$$\alpha_\nu = \sum_i \int n_i(a)\, Q_{i,\nu,e}\, \pi a^2\, da.$$

The interaction of a dusty medium with the radiation field then requires the knowledge of the quantities $Q_{\nu,a}$, $Q_{\nu,s}$ and f_ν. The Mie (1908) theory provides analytic solutions for homogeneous spheres and infinite cilinders. Otherwise, for irregularly shaped and inhomogeneous grains good approximations can be obtained by simple generalizations of the exact solutions for spheres and cylinders (e.g. Hoyle & Wickramasinghe 1991; Bohren and Huffman 1983).

As a source of scattering (like the e^-), another important effect of dust is to induce polarization in the emitted light. Two ways for dust to produce this are through *(a)* light transmission in a dusty medium including oriented bipolar components; or *(b)* dust reflection (e.g. in AGNs). Should we be interested in modelling these effects of dust on polarization, then solutions of the transfer equation (2.1) for all four Stokes parameters would be required.

2.4. Alternative heating mechanisms for dust

Two other heating mechanisms for dust grains can operate (Xu 1997).

(a) Collisional heating for dust mixed with thermal gases. In the HI component of the solar neighbourhood the ratio of collisional heating $G_{\rm coll}$ to radiative heating $G_{\rm rad}$ turns out to be

$$G_{coll}/G_{rad}|_I SRF \simeq v_{HI,thermal}/c;$$

i.e. the collisional is 5 orders of magnitude less than radiative heating! Only in very hot plasmas (IC plasmas at $T > 10^7$) the two can get comparable.

(b) Chemical heating, a process occurring typically in the cold gas component of the ISM, e.g. when an H_2 molecule is formed on the surface of a grain from the combination of 2 H atoms:

$$H + H \rightarrow H_2 + 4.48eV.$$

Most of this chemical energy is absorbed by the grain (the rest is taken by the molecule). The released energy turns out comparable with the collisional one (hence negligible).

2.5. The interstellar extinction curve

Before IRAS, the properties of interstellar dust were mainly inferred from the dimming of optical light of stars inside the Galaxy. If we observe the light from a source through a dust screen, dust emission is negligible in the optical (dust emits significantly only in the IR), offline scattering is unimportant, and the formal solution (eq. 2.1) simplifies to $I_\nu = I_\nu(0)e^{-\tau_\nu}$. Given a source with unextinguished flux $m_\lambda(0)$, the extinction in magnitudes is:

$$A_\lambda \equiv m_\lambda - m_\lambda(0) = \frac{2.5}{\ln 10}\tau_\nu \simeq 1.08\,\tau_\nu.$$

The knowledge of the intrinsic colors for a source population allows to determine the wavelength dependence of the extinction curve. The mean extinction curve along most line-of-sights in the Milky Way has been studied by many authors (see references in Hoyle & Wickramasinghe 1991; and see Figure 1). Its main properties are: *(a)* a growth in the optical-near UV, more than linear with frequency, $\tau \propto \nu^{1.6} \propto \lambda^{-1.6}$ (0.6 - 5 μm); *(b)* a bump around 2175 Å; *(c)* a steeper rise in the far-UV; *(d)* two features in the mid-IR at 9.7 and 18μm.

The extinction curve is not universal: in the Milky Way it depends on the line of sight. Data on other stellar systems (LMC and SMC for example) suggest a variable behaviour, in particular in UV.

More recently it has been possible to evaluate indirectly the extinction curve is distant galaxies, by means of accurate photometric observations in narrow-band filters. Gordon et al. (1997) (see also Calzetti 1997) analyze colour-colour plots for 30

starburst galaxies, inferring starburst ages and extinction properties. The 2175 Å bump is absent and the rise in the far-UV slower than observed for the Milky Way. The authors suggest that the starburst has modified the grain distribution, in particular suppressing the 2175Å feature observed in the MW. Alternatively, Granato et al. (2000) reproduce the observed extinction law in starbursts as a purely geometrical effect, by using the same dust grain mixture than for the MW and accounting for differential extinction for young and old stars (see Sect. 4 below).

2.6. Models of the interstellar dust

The extinction curve, whose main features are reported in Fig. 1, can be explained by a mixture of grains with different sizes and compositions. The curve in the optical is reproduced by grains with $a \sim 0.1\mu$m, while the fast growth of the extinction curve in UV requires smaller particles with $a \sim 0.01\mu$m. Silicate grains explain the 9.7 μm and 18 μm emission features, whose large widths suggest the presence of many impurities (*dirty* or *astronomical* silicates).

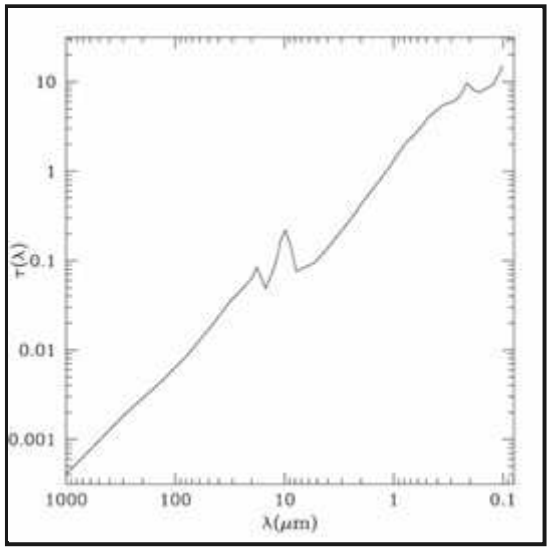

Figure 1. The galactic extinction curve, in optical depth per unit value of E(B - V). The two silicate features at 10 and 18 μm and that of carbonaceous grains at 2175 Å can be recognised.

On the contrary, silicates cannot explain the optical extinction, because of their excessive albedo. Here carbonaceous grains (graphite or amorphous carbon) are proposed as main absorbers, their resonance at 2175 Å nicely fitting the observed UV bump. The non-linear growth in the FUV is probably due to very small grains and PAH molecules (required also to explain the interstellar IR emission bands, e.g. Puget & Leger 1989).

Unfortunately, the extinction curve does not constrain enough the properties of interstellar dust. For this reason, a variety of models, all with the above basic ingredients, have been proposed to reproduce it.

Draine and Lee (1984) adopt a power law size distribution of silicate and graphite grains $dn/da \propto n_H a^{-3.5}$ for $0.005\ \mu m < a < 0.25\mu m$. A quite more complex model by Siebenmorgen & Krugel (1992) includes five classes of grains (amorphous carbon, silicates, very small grains, small PAH and clusters PAH), providing an impressive fit to the extinction curve. The one by Rowan-Robinson (1992) with a discrete set of nine kinds of grain (amorphous carbon size $a = 30\mu m$ and $a = 0.1\mu m$; graphites with $a = 0.03$, 0.01, 0.002 and 0.0005 μm; amorphous silicate $a = 0.1\mu m$ and silicates with $a = 0.03$ and 0.01 μm) explains also the FIR emission from circumstellar envelopes. The population of very big grains is assumed here to explain the sub-mm emission of carbon stars.

The most relevant recent improvement with respect to the classical models by Drain & Lee is the addition to the grain mixture of very small particles and macro-molecules reaching temperatures higher than equilibrium because of their small size, as described above. Two regions of the extinction curve are particularly sensitive to the presence of these small particles: the mid-IR spectrum (including the emission bands at 3.28, 6.2, 7.7, 8.6 and 11.3 μm, and appreciable continuum), and the fast far-UV rise.

The mid-IR emission bands, in particular, are most commonly interpreted as due to a family of very stable planar molecules, the

PAH's (polyciclyc aromatic hydrocarbons), whose vibrational spectra closely resemble, according to laboratory tests, those of emission bands. PAH emission features originate mainly in the so-called *photo-dissociation regions*, i.e. in the interfaces between molecular clouds and the HII regions, where the cloud surfaces are illuminated by the high energy field of the young stars. There are evidences that in denser environments and stronger UV field intensities the PAHs (and the associated mid-IR bands) could be depleted. In the circum-nuclear dusty regions around AGNs PAH emission is not observed.

PAH emission features have been observed by ISO to display Lorentian profiles, whose broad overlapping wings may mimic a kind of continuum (Boulanger et al. 1998). This may possibly explain the observed underlying mid-IR continuum in many astrophysical objects.

3. EVALUATING THE DUST EMISSION SPECTRA

Knowing, or guessing, the optical properties of dust, one can predict the spectra of dusty systems. From a computational point of view, we have to distinguish two cases.

- If the IR dust emission is not self-absorbed (τ_{IR} << 1), the emitted spectrum is simply the volume integral of the local emissivity. An ambient of this kind is the diffuse dust in the IR galactic *cirrus*. Solution of the energy balance equation (2.4) provides the *T* distribution for the various grain species. Since, in particular, $Q_{\nu,(a,\,s)} \sim 1$ in UV and $Q_{\nu,(a,\,s)} \propto a/\lambda^{1.5-2}$ in the far-IR, and considering that the left-hand side is dominated by absorption of UV photons while the right hand by emission at long wavelengths, eq. (2.4) can be re-written for a given grain specie as:

$$I_{bol} = \int J_\nu d\nu \simeq \int B_\nu[T_g(a)]Q_{\nu,(a)}d\nu. \quad (3.5)$$

  Since $\int B_\nu[T_g(a)]d\nu = aT_g^4$ and because of the additional dependence implied by $Q_{\nu,(a)} \propto \nu^{1.5-2} \propto T^{1.5-2}$, the grain equilibrium temperature T_g is found to depend very weakly on the intensity of the local radiation field:

$$T_g \propto (I_{bol}/a)^{1/6}. \quad (3.6)$$

  This implies that dust emission spectra in a variety of galactic environments (from quiescent to actively starbursting galaxies and AGNs) are quite stable and robust, with peak emission mostly confined to the wavelength interval $\lambda_{peak} \simeq$ 100 to 30 μm. Longward of λ_{peak} and after eq. (2.3), dust spectra converge according to the RJ law as

$$I_\nu \propto B_\nu[T_g(a)]Q_{\nu,(a)} \propto \nu^{3.5-4},$$

  in agreement with mm observations of local IRAS galaxies by Andreani & Franceschini (1996) and Chini et al. (1995).

- Otherwise, in the presence of IR-thick media (e.g. dense molecular clouds and dusty torii in AGNs), one is faced by the difficult task to solve the transfer equation. We expect that in thick media the IR spectrum will be erased at the short wavelengths (typically in the near- and mid-IR, but sometimes even in the far-IR) by self-absorption.

3.1. Radiative transfer in thick dusty media

In most practical cases, the radiative transfer equation can be solved only with numerical techniques. We mention in this Section a couple of such approaches quite often used.

3.1.1. *Numerical solutions based on iterative schemes*

A first class of solutions adopt an iterative numerical scheme based on applications of the formal solution of the transfer equation (eq.[2]). This was originally developed for interpreting AGN spectra (Granato & Danese 1994; Pier & Krolick 1992; Granato, Danese & Franceschini 1997), but is useful to treat more generally radiative transfer in thick media. Although the source function can be any kind in principle, we discuss here an application by Granato & Danese for a central point-source and

for a planar and azimuthal symmetry of the dust distribution within a minimum r_m and maximum r_M radii. A condition is set on r_m because of dust sublimation: it cannot be lower than $r_m = L_{46}^{0.5}\ T_{1500}^{-2.8}\ (pc)$ to avoid exceeding an equilibrium grain temperature of T_{gr} = 1500 for graphite and T_s = 1000 for silicates.

The two fields to solve for are the radiation field intensity $I_\nu(r, \Theta, \theta, \phi)$ and the grain temperature distribution $T(r, \Theta)$. The solution is found by representing the field intensity as the contribution of two terms

$$I_\nu = I_\nu^1 + I_\nu^2, \quad (3.7)$$

the first term being the radiation field emitted by the central source and estinguished by the dust, with trivial solution from eq. (2.1):

$$I_\nu^1 = \frac{1}{4\pi}\frac{L_\nu(\Theta)}{4\pi r^2} exp[-\tau_\nu(r,\Theta)], \quad (3.8)$$

$L_\nu(\Theta)$ becoming dependent on direction because of differential extinction, τ being the optical depth to the point (r, Θ, Φ). The second term originates from thermal emission by dust, and may be expressed at the zero-th order as the formal solution (eq. 2.2) of the transfer equation:

$$I_\nu^2(r,\Theta,\theta,\phi) = \int_{(r,\Theta)}^{(\infty,\infty)} S_\nu(r',\Theta') exp[-\tau_\nu(r',\Theta')] d\tau_\nu \quad (3.9)$$

The quantity S_ν is the source function j_ν / α_ν which, if the scattering is isotropic, can be expressed as a weigthed average of the scattering and absorption (Rybicki and Lightman 1979) summed over all grain species:

$$S_\nu = \frac{\sum_i \sigma n [Q_{\nu,a} B_\nu(T) + Q_{\nu,s} J_\nu(r,\Theta)]}{\sum_i \sigma n Q_{\nu,s}} \quad (3.10)$$

The function J_ν is the direction-averaged radiation field intensity $\int I_\nu d\Omega$: this integral obviously includes both contributions to the total intensity in eq. (3.7). Finally, assuming radiative equilibrium for the dust grains, the grain temperature distribution is found from eq. (2.4). The following iterative scheme is used to obtain a solution for I_ν:

(1) the zero-th order approximation for I_ν^1 in eq. (3.7) is obtained from eq. (3.8) given L_ν and the adopted dust distribution;

(2) then a zero-th value for the *T*-field is found from eq. (2.4);

(3) the source function S_ν is then computed from eq. (3.10) including the contribution from thermal dust emission;

(4) after eq. (3.9) the second term I_ν^2 of the radiation field is computed and the total field intensity in eq. (3.7) is updated;

(5) convergence is achieved when e.g. *dT* from one step to the other is less than a small fixed amount. Suitable scaling rules are usually adopted to accelerate the convergence.

3.1.2. ***Monte Carlo solutios***

The advantage of brute-force solutions like a Monte Carlo simulation is that it is better suited to treat complex situations for the geometries of the source function and of the spatial distribution of the absorber. Also velocity fields can be naturally considered in the code to map the kinematical structure of the emission lines (e.g. Jimenez et al. 2000).

The usual approach is to assume a given geometrical distribution for the absorber, possibly including a velocity field, and to generate inside (or outside) it photons according to a given source function (plus a background photon distribution). All these

fields are usually discretized into appropriate spatial grids. Each photons are then followed through the distribution of the absorber, their interaction being ruled by the optical depth, albedo and scattering phase functions at that point. The simplest geometrical distributions adopted are (e.g. Disney et al. 1989; Gordon et al. 1997): *the mixed*, in which the source and absorber are homogeneously distributed; *the shell*, where the source and absorber are separated, typically the former inside and the latter outside acting as a screen. However, much more complex situations can be described this way, up to fully 3D distributions without any symmetries (Jimenez et al. 2000).

4. GENERALIZED SPECTRO-PHOTOMETRIC MODELS OF GALAXIES

Twenty years after the first serious models of stellar population synthesis (Tinsley 1977; Bruzual 1983), the most relevant recent progresses have been the attempts to provide a self-consistent description of the effects of dust (and gas) in galaxy spectra and spectral evolution. We review in this Section some recent efforts of generalized spectral synthesis of galaxies from the UV to the sub-mm, including dust effects (as for both the extinction of the primary optical spectrum, and dust re-radiation at longer λ) in the various galactic environments.

Dust plays an important role in all relevant galactic sites: *(1)* the neutral interstellar medium, whose associated dust is heated by the general radiation field (infrared cirrus, prominent in the 100μm IRAS band); *(2)* the dense cores of molecular clouds, where dust optical-depth is very high and prevents light from very young stars to be observed; *(3)* dust in the external layers of molecular clouds (PRD regions), heated by the interstellar radiation field and OB associations formed in the clouds; *(4)* dust around protostars; *(5)* dust around evolved giants and young planetary nebulae; *(6)* hot dust associated with HII regions.

The inclusion of dust means a dramatic complication of spectro-photometric models: the usual assumption of population-synthesis codes - that the global emission of a whichever complex stellar system is simply the addition of the integrated flux of all components independently on the geometry of the system - is no more valid: not only the extinction process depends in a complex way on the relative distributions of stars and dust, but also dust emission itself, at high dust column densities and according to geometry, may be optically thick.

In principle, accounting for dust effects in detail may require a very complex description of: (1) the physical-chemical-geometrical properties of grains, determining their interactions with the radiation field (e.g. amorphous, porous low-albedo grains vs. highly reflective grains); (2) the chemical composition of the ISM where grains have condensed (which affects the dust composition), given by the integrated contribution of all previously active stellar populations in the galaxy; (3) the modifications that grains and molecules undergo during the course of evolution, i.e. sublimation in strong UV radiation fields, sputtering, etc. (see Sect. 2.2).

These complications of the classical purely stellar evolutionary codes cannot be avoided, if we want a complete and reliable description of physical processes inside galaxies. As we will discuss in later Sections, this turns out to be particularly critical when describing what we called the *active phases* during galaxy evolution: *neglecting dust effects in such cases would bring to entirely wrong conclusions.*

On the other hand, the uncertainties introduced by the large number of new parameters are largely reduced by adopting a multi-wavelength (UV through mm) approach, which balances the unknowns with the number of constraints coming from a wide-band observed spectrum.

4.1 Semi-empirical approaches

A phenomenological approach to a global spectrophotometric description of galaxy evolution was recently discussed by Devriend, Guiderdoni & Sadat (1999). This paper elaborates separately the code for stellar population synthesis from that of dust emission. The former is treated with the most recent prescriptions. The dust emission is schematically represented as the contribution of four different components: the PAH emission features, very small grains, big grains illuminated by the general galactic radiation field (cold dust), and big grains illuminated by young stars in starburst regions. These four components are modelled using typical parameter values for the dust composition, radiation field intensity, mass, etc. Relative normalizations of the four components are finally calibrated using the observed relationship between the IRAS colours of galaxies and the bolometric luminosity.

This approach is quite fast as for computation time (in particular it overcomes the problem of solving the radiative transfer equation), and is particularly useful for statistical analyses of large galaxy databases.

4.2. Detailed self-consistent spectro-photometric models

More physically detailed descriptions of the galactic dust emission are discussed by several teams. These models interface two logical procedures:

- (1) the first is to describe, given a prescription for the IMF, the history of star-formation in the galaxy as a function $\psi(t)$ detailing the mass in stars formed per unit time *t*, the actual gas metallicity *Z*(*t*), the abundances of various elements produced by stars during evolution, and the residual gas fraction *g*(*t*) as a function of time;
- (2) the second step is to sum up, at any galactic age *t*, the fluxes from all populations of stars, by solving the radiative transfer equation taking into account how stars and the residual gas and dust are geometrically distributed.

4.2.1. ***Chemical evolution of the ISM***

While point (1) above is addressed in detail by other contributions to these Book (Bruzual), we remind here a few basic concepts.

A galaxy is usually modelled from the chemical point of view as a single environment where primordial gas flows in according to an exponential law

$$\dot{M}(t) \propto exp(-t/t_{inf}). \quad (4.11)$$

The SFR follows a general Schmidt law

$$\psi(t) = \nu M_g(t)^k \propto g(t)^k \quad (4.12)$$

with the addition of one or more bursts of star-formation to describe starburst episodes possibly triggered by galaxy interactions or mergers. The typically adopted value for *k* is 1. For the initial mass function (IMF) the usual assumption is a Salpeter law

$$d\phi(M) \propto M^{-x} dM, \quad x = 2.35, \; M_{min} < M < M_{max} = 100\ M_\odot \quad (4.13)$$

with typically $M_{\rm min} = 0.1\ M_\odot$ (but higher values may apply for example in the case of starbursts). The observed photometric properties of galaxies of various types and morphologies are reproduced by varying in particular $t_{\rm inf}$ and ν.

Given the above parameters, the solution of the equations of chemical evolution allow to compute at any given galactic time all basic quantities, in particular the functions *g*(*t*) and *Z*(*t*), and then, after eq. (4.12), the number of stars generated at that time with metallicity *Z*(*t*). The integrated spectrum of each stellar generation (Single Stellar Population, SSP) then evolves according to the prescriptions of stellar evolution, defining a 2D sequence (spectral intensity *L*[ν, *t*] vs. frequency ν as a function of time, *t*).

4.2.2. ***Geometrical distributions of gas and stars***

In the model by Silva et al. (1998) three different stellar and ISM components are considered in the generic galaxy: *(a)* star-forming regions, comprising molecular clouds (MC), with young stars, gas and dust in a dense phase, and HII regions; *(b)* young stars escaped from the MC complexes; *(c)* diffuse dust ("cirrus") illuminated by the general interstellar radiation field.

For disk galaxies the adopted geometry is a flattened system with azimuthal simmetry and a density distribution for the 3 above components described by *double exponentials*: $\rho = \rho_0\, exp(-\, r/r_{\rm d})\, exp(-\, |z|/z_{\rm d})$.

For spheroidal galaxies, spherical symmetry is adopted with King profiles $\rho = \rho_0\, ((1 + [r\,/\,r_{\rm c}]^2)^{-\,\gamma} - (1 + [r_{\rm t}/r_{\rm c}]^2)^{-\,\gamma})$, with γ = 3/2,$[r_{\rm t}/r_{\rm c}] \sim 200$, $r_{\rm c} \sim 300pc$ as typical values.

4.2.3. ***Models of the molecular clouds (MC)***

High-resolution CO and radio observations show that MCs are highly structured objects containing very dense cores where stars are actually formed. Typical values for the MCs are: size $\sim$ 10 pc, mass $\sim 10^6\ M_\odot$.

All star-formation in the Galaxy happens in dusty MCs, the early evolution phases of young star clusters occurr inside such dusty regions, hence are optically hidden. Later, on the lifetime of OB stars (10^6 - 10^7 *yrs*), the radiation power of young stars, stellar winds and the first SNs destroy the parent MCs and allow the young stellar population to appear in the optical.

Note that, bacause of the clumpiness of MCs, this is in any case a *statistical process*: in some clouds even the emission of the youngest OB stars is already visible, while in others all young stars are completely embedded in dust. Silva et al. (1998) describe schematically this transition of the MC from a dust-embedded phase to the optically dominated phase, as a process in which the fraction f of the light from the SSP generated within the cloud still embedded into dust decreases linearly with time as $f(t) = 2 - t / t_0$, t_0 being the time interval during which the SSP is entirely extinguished.

The spectrum emitted by the MC and filtered by dust is computed by solving the *transfer equation*, e.g. by assuming that the primary SSP spectrum comes from a point source in the center of the cloud (this rather crude assumption allows substantial semplifications in the numerical code, see above).

A more detailed description of molecular cloud structure and emission is provided by Jimenez et al. (2000). Their model is based on fully three-dimensional simulations of the *density* and *velocity fields* obtained by solving 3D compressible magneto-hydrodynamical (MHD) equations in supersonic turbolent flows, as typical of the motions in Galactic molecular clouds (Padoan et al. 1998). The MHD turbolence generates a large density contrast, with the density field spanning a range of 4 to 5 orders of magnitude. This brings to a *highly filamentary and clumpy morphology*. All this is consistent with observed properties of the clouds.

Young stars with $M > 15 - 20\ M_\odot$ in this model are heavily extinguished for virtually all their live. A detailed Monte Carlo approach is required to solve the radiative transfer equation. The simultaneous knowledge of the density and velocity fields allows also to estimate in great detail the molecular emission lines (CO).

4.2.4. *Models of diffuse dust (cirrus)*

Diffuse dust in the galaxy is responsible for a general attenuation of the light emitted by all stars and MC complexes. In this case the dust column density is not so high to require a detailed solution of the transfer eq. (τ_ν for IR photons is small). One can express an effective optical depth to account for combined absorption and scattering (Rybicky and Lightman 1979): $\tau_{eff} = \tau_a (\tau_a + \tau_s)$. The galaxy is divided into small volume elements V_i, such that the local radiation field in this elementary volume is

$$J(\lambda)_i = \sum_k \frac{V_k [j(\lambda)_k^{mc} + j(\lambda)_k^{star}] e^{-\tau_{eff}(i,k)}}{r_{i,k}^2},$$

$r^2_{i,k}$ being the distance between the i-th and k-th volumes. This determines the temperature of the local diffuse dust, whose integrated flux seen by an observer in a direction θ is a simple sum over all volume elements of the diffuse dust emissivity:

$$S(\lambda,\theta) = 4\pi \sum_k V_k j(\lambda)_k e^{-\tau_{eff}(k,\theta)}$$

τ being the optical depth from the V-element to the outskirts in that direction and $j(\lambda)_k = j(\lambda)_k^{mc} + j(\lambda)_k^{star} + j(\lambda)_k^{cirrus}$.

4.2.5. *Modelling the SEDs of normal and starburst galaxies*

Figure 2 shows the broad-band (UV through radio) spectrum of the prototype starburst galaxy M82, a closeby well studied object at 3.2 Mpc. The lines in the figure come from the fit obtained by Silva et al. (1998). The thin (cyan colored) continuous line peaking at 0.1 μm corresponds to the unextinguished integrated spectrum of all stellar population, while the long-dashed line is the reddened stellar continuum. The dot-dashed line is the contribution of dust in molecular clouds, while the dotted line comes from diffuse dust in the "cirrus". In this model, the optical-NIR spectrum of the galaxy is contributed mostly by old stellar populations unrelated to the ongoing starburst, whereas the starburst emission is mostly observable at $\lambda > 4\ \mu m$ in the form of

dust re-radiation, radio SN and free-free emissions.

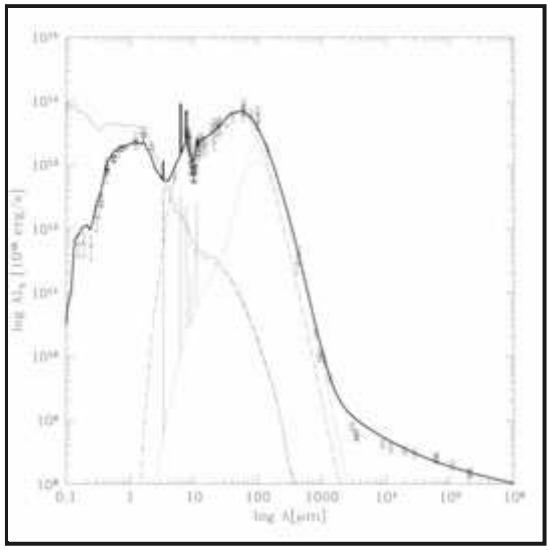

Figure 2. The broad-band (UV through radio) data on the prototype nearby starburst galaxy M82 . The ordinate axis is normalized to 10^{30} *erg/sec*. [Courtesy of G.L. Granato].

Equal areas in the $\lambda L(\lambda)$ plot of Fig. (2) subtend equal amounts of radiant energy: it is then clear from the figure that in this moderate starburst $\sim$ 80% of the bolometric flux emerges as dust re-radiation above 5 μm. In higher luminosity starbursts and in Ultra-Luminous IR Galaxies (ULIRGs, e.g. Arp 220) this fraction gets close to 100%. On the contrary, for local normal galaxies the average fraction is only $\sim$ 30%, as found from comparison of the far-IR with the optical luminosity functions of galaxies (Saunders et al. 1990).

5. INFRARED AND SUB-MM LINE SPECTRA

IR/sub-mm spectroscopy offers unique opportunities to probe the physical conditions ($n[atoms]$, P, T, extinction, ionization state) in the various components of the ISM, because:

- the widespread presence of dust makes optical-UV-NIR line diagnostics completely unreliable;
- most of the line emission by MCs is extinguished and does not appear in the optical;
- lines from molecular phases (including most of the ISM mass) appear in the FIR-mm;
- several fundamental cooling lines of gas happen in the FIR;
- lines from an extremely wide range of ionization states are observable in the IR.

Table 1 summarizes IR tracers of the various ISM components. Clearly, IR spectroscopy is essential for studies of galaxy activity, though it requires a continuous coverage of the IR spectrum, possible only from space. While ISO allowed to invertigate spectroscopically nearby IR active galaxies, future missions (SIRTF, NGST, FIRST) will make possible similar studies for galaxies at any redshifts.

Table 1.Relevant components and line tracers of the ISM

Component	Temperature	Density	Tracers and IR lines
Cold gas	10-100 K	1-1000 cm^{-3}	H_2, CO, PAH's
Diffuse HI	100-1000 K	1 cm^{-3}	HI 21cm, [CII], [OI]
HII regions	1000-10000 K	3-300 cm^{-3}	$H\alpha$, [OII], [OIII]

5.1. The cold molecular gas

Looking at the mm/sub-mm spectral lines is the usual way to study the cold molecular gas, which typically includes the largest mass fraction of the ISM. The lines come from *rotational* and *vibrational* transitions of diatomic and polyatomic molecules.

The very many molecules observable allow to accurately sample the various regimes of ρ, T and elemental abundance.

Unfortunately, the most abundant molecule (H_2) is not easily observed directly. It is seen in absorption in UV, or in the NIR roto-vibrational transitions at 2.121 and 2.247 μm. Only with mid-IR spectroscopy by ISO it was possible to observe the fundamental rotational lines at 17 μm (S[1]), 28.2 μm (S[0]), and 12.3 μm (S[2]) in NGC6946, Arp220, Circinus, NGC3256, NGC4038 / 39). These observations indicate very cool gas to be present with very high column densities (the transition probabilities of the lines are very low).

Because of the difficulty of a direct measure, the amount of molecular gas (H_2) is often inferred from easier measurement of CO emission lines, assumed an H_2/CO conversion. CO rotational transitions allow excellent probes of cold ISM in galaxies: the CO brightness temperature ($\propto$ line intensity) is almost independent on z at z = 1 to 5, due to the additional $(1 + z)^2$ factor with respect to the usual scaling with the luminosity distance (Scoville et al. 1996). CO line measurements have been performed for all IRAS sources in the Bright Galaxy Sample, the majority have been detected with single-dish telescopes. In the most luminous objects the molecular mass is 0.2 - 5 10^{10} $M_\odot$, i.e. 1 to 20 times the content of Milky Way. Typically 50% or more of this mass

is found within the inner kpc from the nucleus, the molecular mass substantially contributing to the total dynamical mass (> 50% of M_{dyn}). Unfortunately, detecting CO emission by high-z galaxies has proven to be difficult (see below).

5.2. The cold neutral gas

The diffuse neutral ISM is commonly traced by the HI 21 cm line from ground-based observations. HI cooling, which is essential to achieve temperatures and densities needed to trigger SF, depends mainly on emission by the 158μm [CII] line, the 21 cm line and the 63μm [OI] line.

The 158 μm [CII] line is a major coolant for the diffuse neutral gas and a fundamental cooling channel for the photo-dissociation regions (PDR's), the dense phase interfacing cold molecular clouds with the HII or HI lower-density gas. Carbon is the most abundant element with ionization potential (11.3 eV) below the H limit (13.6 eV): CII atoms are then present in massive amounts in neutral atomic clouds. The two levels in the ground state of CII responsible for the λ = 158 μm transition correspond to a relatively low critical density $n_{crit} \simeq 300\ cm^{-3}$ [the density at which collisional excitation balances radiative de-excitation]: CII is excited by electrons and protons and cools down by emitting a FIR photon. The CII line intensity is also weakly dependent on T, hence a good measure for P. The [OI]145μm and 63μm lines are also coolants, though less efficient.

5.3. The ionized component of the ISM

Again, a number of lines from atomic species, covering an extremely wide range of ionization conditions, are observable in the far-IR. Their observations allow extensive analyses of the physical state of the gas. This, coupled with the modest sensitivity to dust extinction, provides the ideal tool to probe even the most compact, extinguished sites, e.g. in the inner galactic nuclei.

For a detailed physical investigation, line ratios sensitive to either gas temperature T or density n are used. To estimate electron density n one can use the strong dependence of the fine-structure line intensities for doublets of the same ion on n: one example are the [OIII] lines at 5007 Å, 52 μm and 88 μm. Similarly one can estimate T and the shape of the ionizing continuum.

Particularly relevant to test the spectral shape of the ionizing continuum are the *fine-structure lines from photo-ionized gas*, which allow to discriminate spectra of stellar and quasar origin. Low-ionization transitions typically strong in starbursts are [OIII]52 and 88, [SiII]34, [NeII]12.8, [NeIII]15.6, [SIII]18.7 and 33.4, while higher ionization lines in AGNs are [OIV]25.9 and [NeV]24. Table 2 reports a few of the most important IR ionic lines.

Table 2. The most important IR fine-structure lines. [(a)] Line intensity compared with the observed [CII]158μm for the prototypical starburst M82, when available, or predicted by Spinoglio & Malkan (1992) from a model reproducing the physical conditions in M82.

Species	Excitation potential	λ (μm)	n_{crit} cm^{-3}	F/F[CII][(a)]
OI	-	63.18	$5\ 10^5$	1.4
OI	-	145.5	$5\ 10^5$	0.06
FeII	7.87	25.99	$2\ 10^6$	
SiII	8.15	34.81	$3\ 10^5$	2.6
CII	11.26	157.7	$3\ 10^2$	1
NII	14.53	121.9	$3\ 10^2$	0.37
NII	14.53	203.5	$5\ 10^1$	0.11
ArII	15.76	6.99	$2\ 10^5$	0.11
NeII	21.56	12.81	$5\ 10^5$	2.1
SIII	23.33	18.71	$2\ 10^4$	0.68
SIII	23.33	33.48	$2\ 10^3$	1.1
ArIII	27.63	8.99	$3\ 10^5$	0.23
NIII	29.60	57.32	$3\ 10^3$	0.31
OIII	35.12	51.82	$5\ 10^2$	0.74
OIII	35.12	88.36	$4\ 10^3$	0.66
NeIII	40.96	15.55	$3\ 10^5$	0.16
OIV	54.93	25.87	10^4	-

One important application of IR spectroscopy was by Genzel et al. (1998), to investigate the nature of the primary energy source in IR luminous galaxies (see Sect. 6.8).

6. IR STARBURST AND ULTRA-LUMINOUS GALAXIES IN THE LOCAL UNIVERSE

For a variety of reasons it is unlikely that star-formation (SF) in galaxies has proceeded quietly during the Hubble time. 'A posteriori' evidence has accumulated that a fraction of stars in stellar systems was produced during short-lived events (see e.g. the excellent review in Moorwood, 1996). These SF events are expected to be very luminous, either in the optical or in the IR, and are expected to contribute substantially to the global energetics from baryon thermonuclear reactions, to the synthesis of metals, and the generation of background radiations in the optical, IR and sub-mm. Also the origin of Es, S0s and of the bulges of spirals may have some relationship with luminous and ultra-luminous starburst events at high-z.

If the study of star-formation in high-redshift sources is a primary task for modern cosmology, it is obvious that relevant information for the interpretation of distant objects comes from a close up on local galaxies with enhanced SF. For this reason we consider in this Section a sub-class of local galaxies, *the starburst galaxies and the IR luminous and ultra-luminous galaxies*, including a small fraction (few %) of all local objects, but accounting for a large percentage of the present-day star formation in galaxies.

The discovery of the starburst phenomenon dates back to the 1970's and came almost simultaneously from two quite independent lines of investigation: from objective-plate (Markarian) surveys of UV-excess galaxies, and from the first pioneering IR observations of galaxies in the local universe. IR observations, in particular, revealed the existence of galaxies with IR luminosities and L/M ratios appearently too high to be sustained over their lifetimes (Harwit and Pacini 1975). This brought to the idea that some galaxies undergo a sudden burst of massive star formation, with dust reprocessing of UV photons emitted by the young stars interpreted as the source of the IR light.

From these observations it was clear that SF has a twofold appearence, a UV excess and an IR excess, which may be explained by the *stocastical nature of the interaction between photons and dust* in star-forming regions of galaxies (see above).

However, the abilities of UV and IR surveys to sample the starburst phenomenon are very different: while at low bolometric luminosities UV and IR surveys sample roughly the same kind of objects, at high luminosities the UV flux is no more a good tracer of the SF, which is better sampled by the IR emission. This effect is due to dust extinction of the UV-light by young stars becoming more and more relevant at the higher bolometric luminosities ($L_{bol} > 10^{11}\ L_{\odot}$, Sanders and Mirabel 1996). At the highest values of L_{bol} ($> 10^{12}\ L_{\odot}$) most (> 95%) of the flux comes out in the IR.

L_{bol} is also tightly correlated with the optical morphology: while at low-L there is a "natural" mix of various (mostly late) types, at the higher-L nearly all objects appear to be interacting galaxies, and at the highest-L they look as advanced mergers. Also, the correlation is in the sense that while in low-L objects the SF activity is spread over the galactic disk (enhanced in the spiral arms), at increasing luminosity the SF gets more and more concentrated in the nuclear regions.

In the higher-L objects in particular, it is often observed a concomitant stellar and nuclear non-thermal (AGN) activity, usually the latter occurring in the dynamical center of the galaxy and the former in a circum-nuclear ring (at $\sim 1\ kpc$).

A basic difficulty encountered in studies of active galaxies is to disentangle between starburst-dominated and AGN-dominated energy sources of the IR-luminosity. In fact, the two astrophysical processes are quite often associated in the same object. Optical line ratios (high vs. low excitation, e.g. [OIII]5007 / H β vs. [NII]6583 / H α, the Osterbrock diagram) and line widths (few hundreds Km/s for starbursts, larger for AGNs) are sometimes useful indicators, even in the presence of dust.

Useful near-IR lines, accessible from ground, are the Hydrogen Br γ 2.166μ, HeI2.058μ, H_2, but also higher atomic number species, [FeII] among others. The Br γ 2.166μ and HeI2.058μ, in particular, so close in λ that differential extinction i negligible, constrain the underline ionization spectrum.

However, the most reliable information is provided by mid- and far-IR spectroscopy by space observatories. Extremely promising in this field, in addition to ISO and SIRTF in the next few years, are the planned large space telescopes: NGST in the mid-IR and FIRST in the far-IR.

6.1. The infrared-radio correlation

While there is no direct proof for the basic interpretation of the IR starburst phenomenon (i.e. being due to UV light from newly formed stars absorbed by dust and re-emitted in the IR), an indirect support comes from the well-known radio to far-IR luminosity correlation (de Jong et al. 1985, Helou et al. 1985). This, which is the tightest correlation involving global properties of galaxies, provides an important constraint on the physics ruling starbursts of any luminosities. It not only involves luminous active starbursting galaxies, but also many other galaxies, like quiescent spirals.

The correlation is parametrized by the ratio of the bolometric far-IR flux F_{FIR} (in $erg/s/cm^2$) to the radio flux S_ν (in *erg/s/cm*^{2}*/Hz*):

$$q = log[F_{FIR}/3.75\ 10^{12}\ Hz/S_\nu(1.4\ GHz)] \simeq 2.35, \qquad \sigma(q) \simeq 0.2 \quad (6.14)$$

which is observed to keep remarkably constant with L_{bol} ranging over many orders of magnitude, from low-luminosity spirals up to ultraluminous objects (Arp 220) [small departures from linearity appearing at the low- and high-luminosity ends].

The relation is interpreted as an effect of the ongoing star formation: the far-IR emission comes from dust heated by UV photons by young stars, which also heat the ISM producing free-free emission and generate SN originating high-energy e^- and synchrotron flux mostly by interaction with the general galactic magnetic field. This same scheme explains the departures from linearity: e.g. q slightly increases at the low-luminosity end because L_{FIR} is also contributed by the flux by old stars heating the dust. The radio emission tends to be less concentrated than the far-IR, because of fast e^- diffusion.

6.2. Estimates of the star formation rate (SFR)

As the bolometric luminosity increases, the optical indicators of the SFR (e.g. the UV flux, or the EW of H α) become increasingly uncertain, as a larger and larger fraction of short- λ photons are extinguished. In such a situation, the IR luminosity (proportional to the luminosity by young stars) becomes the most reliable indicator of the SFR. A slight complication here is that older stars illuminating the diffuse cirrus dust in galaxies also contribute to the far-IR flux, particularly in low-luminosity inactive systems.

The SFR is estimated by Telesco (1988) from the energy released by the CNO cycle and assuming a Salpeter IMF (eq. 4.13):

$$SFR(OBA) = 2.1\ 10^{-10}\ L_{FIR}/L_{\odot}\ [M_{\odot}/yr], \quad SFR(All) = 6.5\ 10^{-10}\ L_{FIR}/L_{\odot}\ [M_{\odot}/yr]$$

the former relation referring to the OBA star formation. A refined calibration is given by Rowan-Robinson et al. (1997):

$$SFR(All) = 2.6\ 10^{-10}\ \phi\ \epsilon\ L_{60\mu}/L_{\odot}\ \ [M_{\odot}/yr]$$

where ϕ incorporates the correction from a Salpeter IMF to the true IMF ($\phi \sim 3.3$ going to a Miller-Scalo) and includes corrections for the cut in the IMF (e.g. $\phi \sim 1/3$ if only OBA stars are formed), ϵ being the fraction of photons re-radiated in the IR.

Another mean of estimating the ongoing SFR exploits the radio flux (Condon 1992), by relating the SN rate to the rate of SF and using observations of the radio luminosity of the Milky Way to calibrate the relation. Since the synchrotron emission (proportional to the rate of SN remnant production) and thermal radiation (from HII regions heated by young OB stars) dissipate in 10^7 - 10^8 yrs, the radio flux provides a good measure of the instantaneous SFR. Operatively, one needs to estimate the fraction of stars with masses $M > 8\ M_{\odot}$, progenitors of type-II SN, formed per unit time. The problem with faint radio-source observations is that the radio emission of stellar origin gets easily confused with non-thermal emission by a radio-loud AGN.

Finally, ISO observations indicate that also the mid-IR flux [dominated by hot dust and PDR emission] traces very well the SFR (see Sect. 12.1.2 below).

All these long-wavelength methods provide obvious advantages, in terms of robustness with respect to dust-extinction, compared with the optical ones, namely the relation of SFR with the UV continuum flux by Madau et al. (1996): $SFR(all\ stars) = 5.3\ 10^{-10}\ L_{2800\text{Å}} / L_{\odot}\ [M_{\odot}/yr]$; $SFR(metals) = 1/42\ SFR(stars)$, and that between the $H\alpha$ line flux and the SFR (Kennicut 1998):

$$SFR(all) = 7\ 10^{-42}\ L_{H\alpha}\ [erg/s].$$

Poggianti, Bressan & Franceschini (2000) and Franceschini et al. (2000) have shown that even after correcting for extinction the $H\alpha$ flux using measurements of the Balmer decrement, the $H\alpha$-based SFR is typically a factor ~ 3 lower than the appropriate value inferred from the bolometric flux in IR-luminous galaxies.

Altogether, with these calibrations, moderate luminosity IR starbursts have SFR $\sim$3-30 $[M_{\odot}/yr]$, (corresponding to $\sim 10^5$ O stars present during a typical burst). The most luminous objects, if indeed powered by SF, have SFR up to 1000 $[M_{\odot}/yr]$.

Bolometric flux and SFR are correlated with the broad-band IR to optical luminosity ratio: $L_{IR}/L_B \sim 0.1$ in inactive galaxies (M31, M33), $L_{IR}/L_B \sim 3$ - 10 in luminous ($L \sim 10^{11}\ L_{\odot}$) SBs, $L_{IR} / L_B \sim 100$ in ultra-luminous objects ($L > 10^{12}\ L_{\odot}$, e.g. Arp 220).

6.3. Gas reservoirs, depletion times, starburst duration

The duration of the starburst is critically related with the mass fraction of stars produced during the event and to the available

gas reservoir. Assuming that the SB dominates the spectrum on top of the old stellar population emission, an estimator of the SB duration is the EW of the Br γ line, which is a measure of the ratio of the OB stellar flux (the excitation flux) to the red supergiant star flux (evolved OBA stars). The EW is then expected to evolve monotonically with time. Also, the comparison of the Br γ line with the CO NIR absorption lines is an age indicator (Rieke et al. 1988). Moorwood et al. (1996) find in this way ages of 10^7 to $\sim 10^8$ yrs.

However, *the most direct way to estimate at least an upper limit to the burst duration is the comparison of the total mass of molecular material in the galaxy nucleus with the estimated SFR*, which is also a measure of the efficiency of SF. The gas mass is usually estimated from mm-wave CO line emission and from mm continuum observations of dust emission (assuming suitable conversion factors for H_2/CO and dust/gas). Chini et al. (1995) have found that the two independent evaluations of the molecular mass provide consistent results, showing that luminous IR galaxies are very rich in gas (2×10^9 to 2×10^{10} $M_\odot$).

The ratio L_{IR} / M_{gas} assumes enormously different values in different stages of galaxy activity: in normal inactive spirals L_{IR} / $M_{gas} \sim 5$ ($L_\odot/M_\odot$) (e.g. M31), in moderate starbursts L_{IR} / $M_{gas} \sim 20$ (M82, NGC253), in ultra-luminous IR galaxies L_{IR} / $M_{gas} \sim 200$ (Arp 220), in quasars L_{IR} / $M_{gas} \sim 500$.

A limit to the SB duration is then given by $t_{depletion} = 10^{10}\ M_{gas} / L_{IR}$ *yrs*, ranging from typically several Gyrs for inactive spirals down to a few 10^7 yrs for the more active SBs.

6.4. Starburst-driven super-winds

There are several evidences that extremely energetic outfows of gas are taking place in starbursts: *(a)* from optical spectroscopy, evidence for Wolf-Rayet lines indicative of very young SBs (< 10^7 yrs) and outflow of ionized gas, with velocities up to 1000 Km/s (Heckman, Armus & Miley 1990; Lehnert & Heckman 1996); *(b)* from optical imaging there are evidences of bubbles and cavities left over by large, galactic-scale explosions; *(c)* from X-ray spectroscopy, evidence for plasmas at very high temperatures (up to few KeV), far in excess of what the gravitational field could explain (e.g. Cappi et al. 1999).

These highly energetic processes are interpreted as due to *radiative pressure by massive stars, stellar winds and supernovae explosions* occurring in a small volume in the galaxy core, able to efficiently energize the gas and to produce a dynamical unbalance followed by a large scale outflow of the remaining gas.

This phenomenon has relevant implications. It is likely at the origin of the huge amounts of metals observed in the Intracluster Plasma (ICP) in local galaxy clusters and groups. It should be noted that the estimated Fe metallicity of the outflowing plasma ($\sim$ 0.2 - 0.3 solar, Cappi et al. 1999) is similar to the one observed in the ICP. Also the higher abundances (1.5-2 solar) observed in the 2 archetypal starbursts for α elements (Si, O, Mg) may indicate that type-II SN (those produced by very massive stars, M > 8 $M_\odot$) are mostly responsible (Gibson, Loewenstein & Mushotzky 1997). Similar properties are observed in the hot halo plasmas around elliptical galaxies, also rising the question of a possible relationship of the hyper-luminous IR galaxy phenomenon with the formation of early-type galaxies. Therefore, *the enriched plasmas found in local clusters and groups may represent the fossile records of ancient starbursts of the kind we see in local luminous IR starbursts*.

6.5. Starburst models

More precise quantifications of the basic parameters describing the SB phenomenon require detailed modelling. The first successful attempt accounting in some detail for the observed IR and radio data was by Rieke et al. (1980), who demonstrated that the remarkable properties of M82 and N253 are consistent with SB activity.

Since then, a number of groups elaborated sophisticated models of SBs. These successfully reproduce SB properties assuming exponentially decaying SFRs with burst durations of 10^7 to 10^8 yrs, whereas both instantaneous and long duration bursts are excluded.

An important issue addressed by these models is about the stellar IMF during the burst: Rieke et al. found that assuming for M82 a Salpeter IMF with standard low-M cutoff at 0.1 $M_\odot$ resulted in a stellar mass exceeding the limit implied by dynamical mass evaluations. The problem was resolved by assuming that formation of stars with masses less than a few $M_\odot$ is strongly

suppressed. This result however is not univocally supported by more recent studies of M82: e.g. Leitherer and Heckman (1995) solution is for a 1 to 30 $M_\odot$ IMF.

Interesting constraints on the IMF come in particular from the analysis of CO line kinematics in Arp 220: Scoville et al. (1996) indicate that the dynamical mass, the Lyman continuum, the SFR and the burst timescale can be reconciled by assuming a IMF truncated outside 5 to 23 $M_\odot$, with a SFR $\sim$ 90 $M_\odot/yr$ for stars within this mass range. Altogether, there seem to be fairly

clear indications for a "top-heavy" mass function in the more luminous SBs, as compared with quiescent SF in the Milky Way and in spirals. This has relevant implications for the SFR history in galaxies, the cosmic production of light and of heavy elements.

A very detailed modellistic study of starbursts was given by Leitherer & Heckman (1995) and Leitherer et al. (1999), incorporating all up-to-date improvements in the treatment of stellar evolution and non-LTE stellar atmospheric models. The model successfully explains most basic properties of starbursts, as observed in the optical. Model predictions for a continuous SF over 10^8 yrs and a 1-30 $M_\odot$ Salpeter IMF, normalized to a SFR=1 $M_\odot/yr$ are: bolometric luminosity = 1.3 10^{10} $L_\odot$

number of O stars = 2×10^4; ionizing photon flux (λ < 912Å) = 1.5 10^{53} *photons/sec*; SN rate = 0.02 yr^{-1}; K = -20.5 mag; mass deposition rate = 0.25 $M_\odot/yr$; mechanical energy deposition rate = 6 10^{41} erg/sec. Important outcomes of these papers are

predictions for the EW of most important line tracers of the SF ($H\alpha$, Pa β, Br γ), as a function of the time after the onset of SF

and of IMF shape.

Models of dusty starbursts have been discussed by Silva et al. (1998), Jimenez et al. (2000), Siebenmorgen, Rowan-Robinson & Efstathiou (2000), Poggianti & Wu (2000), Poggianti, Bressan & Franceschini (2001). The latter two, in particular, address the question of the classification and interpretation of optical spectra of luminous IR starbursts: they find that the elusive class of *e(a)* (emission+absorption) spectra, representative of a large fraction (> 50%) of all IR SBs, are better understandable as ongoing active and dusty starbursts, in which the amount of extinction is anti-correlated with the age of the population (the youngest stars are the more extinguished, see also Sect. 4.2.3), rather than post-starburst galaxies as sometimes have been interpreted.

6.6. Statistical properties of active galaxy populations

Statistical properties of SB galaxies provide guidelines to understand the origin and triggering mechanisms of the phenomenon. A fundamental descriptor of the population properties is provided by the Local Luminosity Function (LLF), detailing the distribution of space density as a function of galaxy luminosity in a given waveband.

While the faint luminosity end is important for cosmogonic purposes (providing constraints on the formation models, its flattish shape being roughly similar at all wavelengths), SBs and their complex physics dominate at the bright end of the LLF. Indeed, the latter is observed to undergo substantial changes as a function of λ: if the optical/near-IR LLF's display the classical "Schechter" exponential convergence at high-luminosities (essentially tracing the galaxy mass function), LLF's for galaxies selected at longer wavelengths show flatter and flatter slopes (see Fig. 8 below). This flattening is progressive with λ going from the optical up to 60 μm. When expressed in differential units ($Mpc^{-3}L^{-1}$), the bright-end slope of the 60 μm LLF is $\propto L_{60\mu}^{-2}$, according to the extensive sampling by IRAS (Saunders et al. 1990). Note that this flattening is not due to the contribution

of AGNs at 60 μm, which is modest here and quite more important instead at 12 μm. What is progressively increasing with λ up to λ = 60 μ is the incidence of the starburst contribution to the luminosity: it is the starbursting nature of 60μ selected galaxies responsible for the shape of the LLF.

It is interesting to consider that almost the same slopes $\propto L^{-2}$ are found for all known classes of AGNs, from the luminous radio-galaxies (Auriemma et al. 1977; Toffolatti et al. 1987), to the optical and X-ray quasars (Miyaji, Hasinger & Schmidt 2000; Franceschini et al. 1994b). Also to note is the evidence that the L^{-2} slope for AGNs keeps almost exactly the same at any redshifts, in spite of the drastic increase of the source number-density and luminosity with z due to evolution.

There should be a ruling process originating the same functional law in a wide variety of categories of active galaxies and remarkably invariant with cosmic time, in spite of the dramatic differences in the environmental and physical conditions of the sources. This remarkable behaviour may be simply understood as an effect of the triggering mechanism for galaxy (AGN and starburst) activity: *the galaxy-galaxy interactions (either violent mergers between gas rich objects or encounters triggering a*

slight increase of the activity).

The physical mechanism ruling the process is the variation in the angular momentum $\Delta J/J$ of the gas induced by the interaction, and the consequent gas accretion $\Delta m/m$ in the inner galaxy regions (Cavaliere & Vittorini 2000). Starting for example from a δ -function-shaped LLF, the starburst triggered by the interaction produces a transient increase of L which translates into a distortion of the LF towards the high-L's. Assumed $\Delta m/m$ is ruled by the probability distribution of the impact parameter *b*, it is simple to reproduce in this way the LLF's observed asymptotic shape at the high luminosities.

All this points at the interactions as ruling the probability to observe a galaxy during the active phase.

6.7. Starburst triggering

In normal inactive spirals the disk SFR is enhanced in spiral arms in correspondence with density waves compressing the gas. This favours the growth and collapse of molecular clouds and eventually the formation of stars. This process is, however, slow and inefficient in making stars (also because of the feedback reaction to gas compression produced by young stars). This implies that very long timescales (several Gyrs) are needed to convert the ISM into a significant stellar component.

On the contrary, because of the extremely high compression of molecular gas inferred from CO observations in the central regions of luminous starburst galaxies, SF can proceed there much more efficiently. Both on theoretical and observational grounds, it is now well established that the trigger of a powerful nuclear starburst is due to a galaxy-galaxy interaction or merger, driving a sustained inflow of gas in the nuclear region. This gas has a completely different behaviour with respect to stars: it is extremely dissipative (gas clouds have a much larger cross-section and in cloud collisions gas efficiently radiates thermal energy generated by shocks). A strong dynamical interaction breaks the rotational symmetry and centrifugal support for gas, induces violent tydal forces producing very extended tails and bridges and triggers central bars, which produce shocks in the leading front, and efficiently disperse the ordered motions and the gas angular momentum. *The gas is then efficiently compressed in the nuclear region and allowed to form stars*.

These concepts are confirmed by numerical simulations of galaxy encounters. Toomre (1977) was the first to suggest that ellipticals may be formed by the interaction and merging of spirals. This suggestion is supported by various kinds of morphological features (e.g. tidal tails, rings) observed in the real objects and predicted by his pioneering numerical simulations.

Much more physically and numerically detailed elaborations have more recently been published by Barnes and Hernquist (1992), who model the dynamics of the encounters between 2 gas-rich spirals including disk/halo components, using a combined N-body and gas-dynamical code based on the Smooth Particle Hydrodynamics (SPH). Violent tidal forces act on the disk producing extended tails and triggering central bars, who sweep the inner half of each disk and concentrates the gas into a single giant cloud. The final half-mass radii of gas are much less than those of stars: for an M^* galaxy of $10^{11} M_\odot$, $\sim 10^9 M_\odot$ of gas are compressed within 100-200 pc, with a density of $10^3 M_\odot/pc^3$ (Barnes & Hernquist 1996).

Various other simulations confirm these finding. SPH/N-body codes show in particular that the dynamical interaction in a merger has effects not only on the gas component, but also on the stellar one, where the stars re-distribute following the merging and violent relaxation of the potential.

6.8. Ultra-luminous IR galaxies (ULIRGs)

Defined as objects with bolometric luminosity $L_{\rm bol} \simeq L_{\rm IR} > 10^{12} L_\odot$, they are at the upper rank of the galaxy luminosity function. A fundamental interpretative problem for this population is to understand the primary energy source, either an extinguished massive nuclear starburst, or a deeply buried AGN.

A systematic study of this class of sources was published by Genzel et al. (1998), based on ISO spectroscopy of low-excitation and high-excitation IR lines, as well as of the general shape of the mid-IR SED (the intensity of PAH features vs. continuum emission; see also Lutz et al. 1998). While the general conclusion of these analyses is that star-formation is the process dominating the energetics in the majority of ultraluminous IR galaxies, they have also proven that AGN and starburst activity are often concomitant in the same source. This fact is also proven by the evidence (e.g. Risaliti et al. 2000; Bassani et al. 2000) that many of the ULIRGs classified by Genzel et al. as starburst-dominated also show an hidden, strongly photoelectrically absorbed, hard X-ray spectrum of AGN origin. Soifer et al. (2000) have also found that several ULIRGs show very compact (100-300 pc) structures dominating the mid-IR flux, a fact they interprete as favouring AGN-dominated emission. The relative role of SF and AGN in ULIRGs is still to be quantified, hard X-ray (spectroscopic and imaging) observations by CHANDRA and XMM, as

well as IR spectroscopy by space observatories (SIRTF, FIRST) will provide further crucial information.

6.9. Origin of elliptical galaxies and galaxy spheroids

As pointed out for the first time by Kormendy & Sanders (1992), the typical gas densities found by interferometric imaging of CO emission in ultra-luminous IR galaxies turn out to be very close to the high values of stellar densities in the cores of E/S0 galaxies. This is suggestive of the fact that ULIRG's have some relationships with the long-standing problem of the origin of early-type galaxies and spheroids.

Originally suggested by Toomre (1977), the concept that E/S0 could form in mergers of disk galaxies immediately faced the problem to explain the dramatic difference in phase-space densities between the cores of E/S0 and those of spirals. Some efficient dissipation is required during the merger, which can be provided by the gas. Indeed, the CO line observations in ULIRG's, also combined with those of the stellar nuclear velocity dispersions and effective radii, show them to share the same region of the "cooling diagram" occupied by ellipticals.

Detailed analyses of the H_2 NIR vibrational lines in NGC 6240 and Arp 220 (van der Werf 1996) have provided interesting information about the mass, kinematics, and thermodynamics of the molecular gas. The conclusion is that shocks, the fundamental drivers for dissipation, can fully explain the origin of the H_2 excitation. The evidence that the H_2 emission is more peaked than stars, and located in between the two merging nuclei, is consistent with the fact that gas dissipates and concentrates more rapidly, while stars are expected to relax violently and follow on a longer timescale the new gravitational potential ensuing the merger.

A detailed study of Arp 220 by van der Werf (1996) has shown that most of the H_2 line emission, corresponding to $\sim 2 \times 10^{10} M_\odot$ of molecular gas, comes from a region of 460 pc diameter, the gas mass is shocked at a rate of $\sim 40\ M_\odot/yr$, not inconsistent with a SFR $\sim$ 50 - 100 $M_\odot/yr$ as discussed in Sect. 6.5. Compared with the bolometric luminosity of Arp 200, this requires a IMF during this bursting phase strongly at variance with respect to the Salpeter's one (eq. 4.13) and either cut at $M_{min} > > 0.1\ M_\odot$ or displaying a much flatter shape.

In support of the idea that ellipticals may form through merging processes there is evidence coming from high-resolution K-band imaging that the starlight distribution in hyper-luminous IR galaxies follows a de Vaucouleurs $r^{-1/4}$ law typical of E/S0 (Clements & Baker 1997).

Also proven by simulations, after the formation of massive nuclear star clusters from the amount of gas (up to $10^{10}\ M_\odot$) collapsed in the inner Kpc, part of the stellar recycled gas has low momentum and further contracts into the dynamical center, eventually producing a super-massive Black Hole with the associated AGN or quasar activity (Norman and Scoville 1988, Sanders et al. 1988).

7. IR GALAXIES IN THE DISTANT UNIVERSE: PRE-ISO/SCUBA RESULTS

We have summarized in previous paragraphs the main properties of local galaxies when observed at long wavelengths, and emphasized the unique capability of these observations to unveil classes of sources, unnoticeable at other wavelengths, but extremely luminous in the IR. It was clear from this that the most luminous objects in the universe and the most violent starbursters can be reliably studied only at these wavelengths.

Our previous discussion has also illustrated the complexity and difficulty of modelling the long-wavelength spectra of galaxies, heavily dependent on the relative geometries of stars and dust.

Now, assumed we have a decent understanding of the local universe and its IR galaxy populations, we dedicate the next Sections to illustrate and discuss new emerging facts about their distant counterparts, which entail important discoveries for cosmology.

The IRAS survey in 1983, allowing the first sensitive all-sky view of the universe at long wavelengths, is considered as the birth date of IR astronomy. Most of our knowledge about local IR galaxies, as previously discussed, comes from the IRAS database. The fair sensitivity of the IRAS surveys, coupled with the prominent emission of IR galaxies at 60-100 μm, have also allowed to sample and study galaxies at cosmological distances and to derive first tentative indications for evolution.

Counts of IRAS galaxies (mostly at 60 μm, where the S/N was optimum, S including the source signal and N the instrumental and sky [cirrus] noise) have been obtained by Hacking & Houck (1987), Rowan-Robinson et al. (1991), Gregorich et al. (1995), Bertin, Dennefeld, Moshir (1997). Samples at 60 μm with optical identifications and radial velocities have been published by Saunders et al. (1990, 1997), Lonsdale et al. (1990), and Oliver et al. (1996).

Early evidence in favour of evolution for IRAS-selected galaxies have been discussed by Hacking et al. (1987), Franceschini et al. (1988) and Lonsdale et al. (1990), among others. In the models by Franceschini et al. and Pearson & Rowan-Robinson (1996), a sub-population of starburst galaxies including a substantial fraction (30%) of all galaxies in the local universe evolves as $L(z) = L(0)(1 + z)^{3.1}$ (Pearson & Rowan-Robinson) or $L(z) = L(0)e^{4.3\,\tau(z)}$ (Franceschini et al.), roughly reproducing counts and redshift distributions.

However, the IRAS sensitivity was not enough to detect galaxies at substantial redshifts, apart from a handful of exceptions (essentially due to gravitational lensing amplifying the flux): the most distant were found at $z \simeq 0.2$ - 0.3. Any conclusions based on IRAS data are to be considered as preliminary, large-scale inhomogeneities badly affecting these shallow samples.

Another problem for the IRAS surveys was the uncertain identification with faint optical counterparts, because of the large [$\sim 1\ arcmin^2$] IRAS error-box: this implied a systematic bias towards associating IRAS sources with the brightest galaxy falling inside it, which may systematically miss the fainter higher-redshift correct identification.

8. THE BREAKTHROUGHS: DISCOVERY OF THE CIRB

Cosmological background radiations are a fundamental channel of information about cosmic high-redshift sources, particularly if, for technological limitations, observations of faint sources in a given waveband are not possible. This was clearly the case for the IR/sub-mm domain. The present Section is dedicated to a review on a recently discovered new cosmic component, the cosmological background at IR and sub-millimetric wavelengths (CIRB), an important achievement made possible by the NASA's Cosmic Background Explorer (COBE) mission.

To appreciate the relevance of this discovery (anticipated by a detailed modellistic prediction by Franceschini et al. 1994), consider that extragalactic backgrounds at other wavelengths contain only modest (undiscernible) contributions by distant galaxies. The Radio background is clearly dominated by radio-loud AGNs; the Cosmic Microwave Background includes photons generated at $z \sim 1500$; the X-ray and γ-ray backgrounds are dominated by distant quasars and AGNs. Also, diffuse light in the optical-UV (and partly the near-IR) will be hardly depurated of the foreground contaminations (in particular, Galactic starlight reflected by high latitude "cirrus" dust, and Zodiacal-reflected Sun-light).

On the other hand, the recently completed third experiment (DIRBE) of the COBE mission has brought to the *first detection ever (with surprisingly small uncertainties) of the integrated emission of distant galaxies* in the form of an isotropic signal in the far-IR and sub-mm (Puget et al. 1996, Guiderdoni et al. 1997, Hauser et al. 1998, Fixsen et al. 1998).

8.1. Observational status about the CIRB

In spite of the presence of very bright foregrounds (Zodiacal and Interplanetary dust emission, Galactic Starlight, high-latitude "cirrus" emission), relatively clean spectral windows exist in the IR suitable for extragalactic research: the near-IR cosmological window (2-4 μm) and the sub-mm window (100-500 μm). At these wavelengths the Zodiacal, Starlight, and emission by high galactic latitude dust produce two minima in the total foreground intensity, which is much lower here than it is in the optical-UV.

These spectral windows occur where we would expect to observe the redshifted photons from the two most prominent galaxy emission features: the stellar photospheric peak at $\lambda \sim 1\ \mu m$ and the one at $\lambda \sim 100\ \mu m$ due to dust re-radiation. The best chances to detect the integrated emission of distant and primeval galaxies are here.

For a curious coincidence, the (expected) integrated emission of distant galaxies turns out to be comparable by orders of magnitude to the Galaxy emission at the Pole and to the Zodiacal light in the near-IR window. This implies that a delicate subtraction of the foreground emissions is required to access the extragalactic domain.

Three main observational routes have been followed to measure the CIRB:

- rocket flights of dedicated instrumentation (1970-1990), now only of historical interest;
- all-sky surveys by space telescopes (IRAS and COBE, 1984-1996);

- indirect estimates based on very high-energy spectral observations of extragalactic γ-ray sources (Stecker, de Jager & Salomon 1992; Stanev & Franceschini 1998).

In sky directions outside obvious Galactic sources, like star-forming and low-galactic latitude regions, the total far-IR background is due to the contribution of various dust components in the ISM: galactic dust associated with neutral and ionized hydrogen, the interplanetary dust emission, all adding to the isotropic diffuse flux, the CIRB. The way to subtract these various foregrounds when estimating the CIRB intensity is to exploit the different spatial dependencies of the various components, using the correlations with appropriate dust tracers like the HI 21 cm or H_α lines.

To subtract the most important foreground in the far-IR, the galactic dust emission, the simplest procedure is to determine the parameters of the correlation between the background intensity I_ν and the dust tracers expressed in terms of equivalent hydrogen column density N_H, and then to evaluate the CIRB as the intercept of the total flux at $N_H = 0$.

Another method is to perform an all-sky best-fit analysis of a relation like $I_\nu = C_1 N_H(HI) + C_2 N_H(II) + CIRB$, N_H being the column densities of the dust components associated with the neutral and ionized H, *CIRB* being the extragalactic background intensity at the working wavelength (e.g, Lagache et al. 1999). The best-fitting determines the constant C_1 and C_2 and allows to estimate a value for the parameter *CIRB*.

Puget *et al.* (1996) first recognized in the all-sky FIRAS/COBE maps an isotropic signal (independent of Galactic coordinates) with an intensity that can be represented by the law $\nu B_\nu \simeq 3.4 \times 10^{-9} (\lambda/400\mu m)^{-3}\ W\, m^{-2}\, sr^{-1}$ in the 400-1000 μm interval.

This tentative detection has been later confirmed with independent analyses by various other groups (e.g. by Fixsen et al. 1998, who find significant isotropic signal from 200 and 1000 μm), as well as by analyses of data from the DIRBE experiment on COBE in two broad-band channels at λ = 140 and 240μ (Hauser et al. 1998). Finkbeiner, Davies & Schlegel (2000), after a very delicate subtraction of the far dominant Galactic and IPD foregrounds, found an isotropic signal at 60 and 100 μm with intensity at the level of $\sim$ 30 10^{-9} $W\ m^{-2}\ sr^{-1}$. This latter result is presently under discussion, but appears to conflict with independent estimates (see Sect. 8.2).

Recent analyses by Dwek & Arendt (1998) and Gorjian, Wright & Chary (2000) have tentatively found also a signal in the near-IR cosmological window at 3.5 μm and in the J, H and K DIRBE bands, however with large uncertainties because of the problematic evaluation of the Zodiacal (scattered) light. Because of this, CIRB estimates particularly in J, H and K are to be taken more reliably as upper limits.

To avoid overcrowding, we report in Figure 3 only the most recent results from DIRBE (Lagache et al. 1999; Finkbeiner, et al. 2000) and FIRAS (Fixsen et al. 1998).

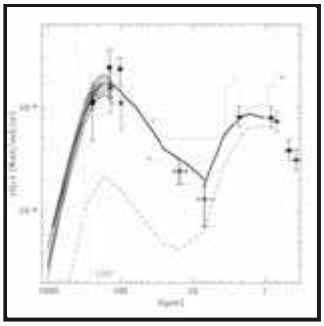

Figure 3. The Cosmic Infrared Background (CIRB) as measured by independent groups in the all-sky COBE maps (e.g. Hauser et al. 1998), compared with the optical extragalactic background estimated from ultradeep optical integrations by the HST in the HDF (Madau & Pozzetti 2000). Three datapoints in the far-IR are from a re-analysis of the DIRBE data by Lagache et al. (1999), the shaded area from Fixsen et al. (1998) and Lagache et al. The two mid-IR points are the resolved fraction of the CIRB by the deep ISO surveys GITES, while dashed lines are limits set by TeV cosmic opacity (Sect. 8.2). The dotted line marks the expectation based on the assumption that the IR emissivity of galaxies does not change with cosmic time. The thick line is the predicted CIRB intensity by the model discussed in Sect. 11.

No isotropic signals are significantly detected at $4\mu < \lambda < 60\mu$, any cosmological flux being far dominated here by the Zodiacal light, the Interplanetary dust (IPD) emission and by Galactic dust emission (only missions to the outer Solar System would have chances to reduce the dominant IPD flux to achieve detection of the CIRB here). The constraints we report at these wavelengths come from indirect estimates based on the cosmic high-energy opacity (Sect. 8.2 below).

Altogether, after four years of very active debate among various teams working on the COBE data, first about the existence and later on the intensity and spectral shape of CIRB, there is now ample consensus even on details of CIRB's spectral intensity, at least from 140 to 300 μm where it is most reliably measured and where two completely independent datasets (FIRAS and DIRBE, with independent absolute calibrations) are available. The CIRB flux has in particular stabilized at values $\nu I_\nu \simeq$ 24±5 and $\nu I_\nu \simeq$ 15±5 10^{-9} $Watt/m^2/sr$ at λ = 140 and 240 μm. Modest differences in the absolute calibration of FIRAS and DIRBE around 100 μ have been reported (Hauser et al. 1998), but these do not seem to affect the overall result.

This was a fundamental achievement for observational cosmology, providing the global energy density radiated by cosmic sources at any redshifts. Two concomitant facts, the very strong K-correction for galaxies in the far-IR/sub-mm implied by the very steep and featureless dust spectra, and their relative robustness due to the modest dependence of dust equilibrium temperature T on the field intensity (eq. 3.6]) have suggested to use the CIRB spectrum to infer the evolution of the galaxy long-wavelength emissivity as a function of redshift (Gispert, Lagache & Puget 2000). Indeed, while the peak intensity at λ = 100 to 200 μm constrains the galaxy emissivity at z = 0 to z = 1, the quality of the FIRAS intensity maps and the low foreground contamination at $\lambda > 200\ \mu m$ allow to set important constraints on the universal emissivity at $z > 1$.

Between 100 and 1000 μm the integrated CIRB intensity turns out to be $\sim$ 30±5 10^{-9} $Watt/m^2/sr$. In addition to this measured part of the CIRB, one has to consider the presently un-measurable fraction resident in the frequency decade between 100 and 10 μm. This flux is larger than the integrated "optical background" ($\sim$ 17 $nWatt/m^2/sr$, see Fig. 3), obtained by counting all galaxies detected between 0.3 and 3 μm by HST down to the faintest detectable sources. This procedure to estimate the "optical

background" relies on the fact that optical counts show a clear convergence at magnitudes $m_{AB} \geq 22$ (Madau & Pozzetti 2000), such that the expected contribution by sources fainter than HST limiting fluxes appears negligible (a significant upwards revision of this optical background suggested by Bernstein et al. [1998] to account for low surface brigtness emission by galaxies is not confirmed).

Already the directly measured part of the CIRB sets a relevant constraint on the evolution of cosmic sources, when compared with the fact mentioned in Sect. 4.2.5 that for local galaxies only 30% of the bolometric flux is absorbed by dust and re-emitted in the far-IR. *The CIRB's intensity matching or even exceeding the optical background tells unequivocally that galaxies in the past should have been much more "active" in the far-IR than in the optical, and very luminous in an absolute sense. A substantial fraction of the whole energy emitted by high-redshift galaxies should have been reprocessed by dust at long wavelengths.*

8.2. Constraints from observations of the cosmic high-energy opacity

As originally suggested by F. Stecker soon after the discovery of high-energy photon emissions from distant blazars, high-energy spectral observations may provide a suitable alternative to the direct detection of the CIRB at wavelengths where it is currently impossible. The idea is to infer the CIRB intensity from combined GeV and TeV observations of a set of Blazars by exploiting the $\gamma \rightarrow \gamma$ interaction of their emitted high energy photons with those of the CIRB.

The absorption cross-section of γ-rays of energy E_γ [TeV] has a maximum for IR photons with energies obeing the condition (Stecker, de Jager & Salomon 1992):

$$\epsilon_{max} = 2(m_e c^2)^2 / E_\gamma,$$

which implies

$$\lambda_{peak} \simeq 1.24 \pm 0.6 (E_\gamma [TeV])\ \mu m. \quad (8.15)$$

The optical depth for a high-energy photon E_0 travelling through a cosmic medium filled of low-energy photons with density $\rho(z)$ from z_e to the present time is

$$\begin{aligned} \tau(E_0, z_e) &= c \int_0^{z_e} dz \frac{dt}{dz} \int_0^2 dx \frac{x}{2} \int_0^\infty d\nu (1+z)^3 \frac{\rho_\nu(z)}{h\nu} \sigma_{\gamma\gamma}(s) \\ \sigma_{\gamma\gamma}(s) &= \frac{3\sigma_T}{16}(1-\beta^2)[2\beta(\beta^2-2) + (3-\beta^4) ln(\frac{1+\beta}{1-\beta})] \\ s &\equiv 2E_0 h\nu x (1+z); \quad \beta \equiv (1 - 4m_e^2 c^4/s)^{1/2}. \end{aligned} \quad (8.16)$$

Coppi & Aharonian (1999) report the following analytical approximation, good to better than 40%, to eq. (8.16):

$$\tau(E_0, z_e) \simeq 0.24 \frac{E_\gamma}{TeV} \frac{\rho(z=0)}{10^{-3} eV/cm^3} \frac{z_e}{0.1} h_{60}^{-1} \simeq 0.063 \frac{E_\gamma}{TeV} \frac{\nu I_\nu}{nW/m^2/sr} \frac{z_e}{0.1} h_{60}^{-1} \quad (8.17)$$

Interesting applications of this concept have been possible when data from the Compton Gamma Ray Observatory and from hard X-ray space telescopes have been combined with observations at TeV energies by the Whipple and other Cherenkov observatories on the Earth.

Stanev & Franceschini (1998) have obtained model-independent upper limits on the CIRB with no a-priori guess about the CIRB spectrum, using HEGRA data for the Blazar MKN 501 (z = 0.034) during an outburst in 1997, on the assumption that the high-energy source spectrum is the flattest allowed by the data. These limits (see Fig. 3) get quite close to the CIRB background already resolved by the ISO mid-IR deep surveys (see Sect. 9).

More recently, Krawczynski et al. (1999) have combined the observations of MKN501 during the 1997 outburst with X-ray data from RossiXTE and BeppoSAX, providing a simultaneous high-quality description of the whole high-energy spectrum. These data are very well fitted by a Synchrotron Self Compton (SSC) model in which the spectrum at $\nu = 10^{27} Hz$ is produced by Inverse Compton of the hard X-ray spectrum at $\nu = 10^{18} Hz$: the combination of the two provides solid constraints on the shape of the "primary" (i.e. before cosmic attenuation) spectrum at TeV energies. This is used to derive $\tau_{\gamma\gamma}$ as a function of energy and, after eqs. 8.16 and 8.17, a constraint on the spectral intensity of the CIRB. The result is compatible with the limits by Stanev & Franceschini (1998) and allows to get a tentative estimate of the CIRB intensity in the interval from $\lambda = 10$ to $40\ \mu m$ (see Fig. [3]), which is formally dependent, however, on the SSC model adopted for the intrinsic source spectrum.

Less model dependent is the constraint set by the observations of purely power-law Blazar spectra around $E_\gamma \simeq 1\ TeV$, which translates into the upper limit of about 10 $nanoWatt/m^2/sr$ at $\lambda \simeq 1\ \mu m$ shown in Fig. 3. Substantially exceeding that, as suggested by some authors (Bernstein et al., Gorjian et al.), would imply either very "ad hoc" γ -ray source spectra or new physics (Harwit, Proteroe & Bierman 1999).

8.3. Contribution of cosmic sources to the CIRB: the formalism

A simple formalism relates background intensity and cell-to-cell anisotropies to the statistical properties (luminosity functions and number counts) of the contributing sources.

8.3.1. ***Source contribution to the background intensity***

The differential number counts (sources/unit flux interval/unit solid angle) at a given flux S write:

$$\frac{dN}{dS} = \int_{z_l}^{z_h} dz \frac{dV}{dz} \frac{d\log L(S;z)}{dS} \rho[L(S,z),z] \quad (8.18)$$

where $\rho[L(S,\ z),\ z]$ is the epoch-dependent luminosity function and dV/dz is the differential volume element. Flux S and rest-frame luminosity L are related by

$$S_{\Delta\nu} = \frac{L_{\Delta\nu} K(L,z)}{4\pi d_L^2}, \quad (8.19)$$

where d_L is the luminosity distance and $K(L,\ z) = (1 + z)\ \frac{L[\nu(1+z)]}{L(\nu)}$ the K-correction. The contribution of unresolved sources (sources fainter than the detection limit S_d) to the background intensity is given by:

$$I = \int_0^{S_d} \frac{dN}{dS} S\, dS = \frac{1}{4\pi} \frac{c}{H_0} \int_{z(S_d, L_{\min})}^{z_{\max}} \frac{dz}{(1+z)^6 (1+\Omega z)^{1/2}} j_{\rm eff}(z), \quad (8.20)$$

having defined the volume emissivity $j_{\rm eff}(z)$ as

$$j_{\rm eff}(z) = \int_{L_{\min}}^{\min[L_{\max}, L(S_d,z)]} d\log L\ L\ n_c(L,z) K(L,z), \quad (8.21)$$

where $L_{\min}$ and $L_{\max}$ are the minimum and the maximum source luminosities. From eq. (8.20) we can note that, when the counts converge like $dN/dS \propto S^{-2}$ or flatter, the contribution by faint sources to the background intensity becomes almost insensitive to the source minimum flux [$I \propto ln(S_{\min})$ or less]. This property has been used by Madau & Pozzetti (2000) to estimate the optical background intensity (see Fig. 3) from ultra-deep HST counts of galaxies, by exploiting the convergence of the optical counts

fainter than $m_{AB} \sim 22$. A similar property of faint IR sources is used in Sect. 9.4 to estimate the contribution of IR galaxies to the CIRB.

8.3.2. ***Small scale intensity fluctuations***

In addition to the average integrated flux by all sources in a sky area, the background radiation contains also spatial information (the cell-to-cell fluctuations) which can be used to further constrain the source flux distribution and spatial correlation properties (e.g. De Zotti et al. 1996). The usually most important contribution to the cell-to-cell intensity fluctuations comes from the stochastic nature of the spatial distribution of sources among elementary cells with an effective solid angle $\omega_{\rm eff,P}$ (Poisson fluctuations). They can be expressed as

$$(\delta I)^2 \equiv C(0) = \frac{\omega_{\rm eff,P}(0)}{4\pi} \int_0^{S_d} S^2 \frac{dN}{dS} dS. \quad (8.22)$$

What is really measured, however, is not the flux S but the detector's response $x = f(\vartheta, \varphi)S$, $f(\vartheta, \varphi)$ being the angular power pattern of the detector. Let $R(x) = \int dN \left[x / f(\vartheta, \varphi) \right] / dS \cdot d\omega / f(\vartheta, \varphi)$ be the *mean number of source responses* at *intensity* x. For a Poisson distribution of the number of sources producing a response x, its variance equals the mean $R(x)dx$. Adding the variances of all responses up to the cutoff value x_c (brighter sources are considered to be individually detected) gives the contribution of unresolved sources to fluctuations:

$$(\delta I)^2 = \int_0^{x_c} x^2 R(x)\, dx. \quad (8.23)$$

The cutoff x_c is chosen to be some factor q times $(\delta I)^2$; usually q = 3-5. The rms background fluctuations (δI) imply a sky noise $\sigma_{conf} = \langle (\delta I)^2 \rangle^{1/2}$ for observations with spatial resolution ω_{eff}.

The integrated signal D recorded by the detector is the sum of the responses x due to all sources in the angular resolution element. Its probability distribution function $P(D)$ is informative on the amplitude and slope of counts of unresolved sources. Scheuer (1957) has shown that its Fourier transform, $p(\omega)$, is a simple function of the FT $r(\omega)$ of $R(x)$: $p(\omega) = \exp[r(\omega) - r(0)]$. It follows:

$$P(D) = \int_{-\infty}^{\infty} p(\omega) \exp(-2\pi i \omega D)\, d\omega = \int_{-\infty}^{\infty} \exp\left[r(\omega) - r(0) - 2\pi i \omega D\right] d\omega =$$
$$2 \int_0^{\infty} \exp\left\{ - \int_0^{\infty} R(x) \left[1 - \cos(2\pi\omega x)\right] dx \right\} \cdot \cos\left[\int_0^{\infty} R(x) \sin(2\pi\omega x)\, dx - 2\pi\omega D \right] d\omega. \quad (8.24)$$

This synthetic $P(D)$ has to be convolved with the noise distribution to be compared with the observations. Assumed that the number count distribution below the detection limit can be represented as a power-law, $N(>S) = K(S / S_k)^{-\beta}$, then eq. [8.24] can be integrated to get (Condon 1974):

$$\sigma_{conf} = \left[\frac{q^{2-\beta}}{2-\beta} \right]^{1/\beta} (\omega_{eff} \beta K)^{1/\beta} S_k, \qquad \omega_{eff} = \int f(\vartheta, \varphi)^{\beta} d\Omega \quad (8.25)$$

which allows to estimate the slope of the counts (β) below the detection limit from a given measured value of the cell-to-cell fluctuations σ_{conf}. This constraint on $N(S)$ applies down to a flux limit corresponding to $\sim$ 1 source/beam. Assumed that S_k represents the confusion limit ($S_k = q \times \sigma_{conf}$) of a survey having an areal resolution ω_{eff}, then eq. 8.25 further simplifies to

a relation between the number of sources K resolved by the survey (and brighter than S_k) and the parameters q and β:

$$K = \frac{2-\beta}{\beta q^2}\frac{1}{\omega_{eff}} : \quad (8.26)$$

this implies the confusion limit to occur at the flux corresponding to an areal density of (βq^2/[2 - β])$^{-1}$ sources per unit beam area ω_{eff} . For euclidean counts and q = 3, this corresponds to 1 source/27 beams. Confusion limits based on this criterion for various IR observatories are indicated in Figs. 6 and 7 below.

9. DEEP SKY SURVEYS WITH THE INFRARED SPACE OBSERVATORY (ISO)

ISO has been the most important IR astronomical mission of the 1990s. Launched by ESA, it consisted of a 60 cm telescope operative in a highly eccentric 70000 Km orbit. It included two instruments of cosmological interest (in addition to two spectrographs): a mid-IR 32×32 camera (ISOCAM, 4 to 18 μm), and a far-IR imaging photometer (ISOPHOT, with small 3×3 and 2×2 detector arrays from 60 to 200 μm). The whole payload was cooled to 2 K by a He^3 cooling system so performant to allow ISO to operate for 30 months (Nov 1995 to Apr 1998), instead of the nominal 18 months. An excellent review of the extragalactic results from ISO can be found in Genzel & Cesarsky (2000).

9.1. Motivations for deep ISO surveys

While designed as an observatory-type mission, the vastly improved sensitivity offered by ISO with respect to the previous IRAS surveys motivated to spend a relevant fraction of the observing time to perform a set of deep sky explorations at mid- and far-IR wavelengths. The basic argument for this was to parallel optical searches of the deep sky with complementary observations at wavelengths where, in particular, the effect of dust is far less effective in extinguishing optical light. This could have been particularly relevant for investigations of the distant universe, given the large uncertainties implied by the (pobably large) extinction corrections in optical spectra of high redshift galaxies (e.g. Meurer et al. 1997).

Observations in the mid- and far-IR also sample the portion of the e.m. spectrum dominated by dust re-processed light, and are then ideally complementary to optical surveys to evaluate the global energy output by stellar populations and active nuclei.

Organized in parallel with the discovery of the CIRB, a major intent of the deep ISO surveys was to start to physically characterize the distant sources of the background and to single out the fraction contributed by nuclear non-thermal activity in AGNs.

Finally, exploring the sky to unprecedented sensitivity limits should have provided an obvious potential for discoveries of new unexpected phenomena from our local environment up to the most distant universe.

9.2. Overview of the main ISO surveys

Deep surveys with ISO have been performed in two wide mid-IR (LW2: 5-8.5μm and LW3: 12-18μm) and two far-IR (λ_{eff} = 90 and 170 μm) bands. The diffraction-limited spatial resolutions were $\sim$5 arcsec at 10 μm and $\sim$50 arcsec at 100 μm. Mostly because of the better imaging quality, ISO sensitivity limits in the mid-IR are 1000 times better than at the long wavelengths (0.1 mJy versus 100 mJy). At some level the confusion problem will remain a fundamental limitation also for future space missions (SIRTF, FIRST, ASTRO-F). A kind of compensation to these different performances as a function of λ derives from the typical FIR spectra of galaxies and AGNs, which are almost typically one order of magnitude more luminous at 100 μm than at 10 μm. We detail in the following the most relevant programs of ISO surveys.

9.2.1. *The ISOCAM Guaranteed Time (GT) Extragalactic Surveys*

Five extragalactic surveys with the LW2 and LW3 filters have been performed in the ISOCAM GT (GITES, P.I. C. Cesarsky), including large-area shallow surveys and small-area deep integrations. A total area of 1.5 square degrees in the Lockman Hole and the "Marano" southern field have been surveyed, where more than one thousand sources have been detected (Elbaz et al. 1999). These two areas were selected for their low zodiacal and cirrus emissions and because of the existence of data at other wavelengths (optical, radio, X).

9.2.2. *The European Large Area ISO Survey (ELAIS)*

ELAIS is the most important program in the ISO Open Time (377 hours, P.I. M. Rowan-Robinson, see Oliver et al. 2000a). A total of 12 square degrees have been surveyed at 15 μm with ISOCAM and at 90 μm with ISOPHOT, 6 and 1 sq. degrees have been covered with the two instruments at 6.7 and 170 μm. To reduce the effects of cosmic variance, ELAIS was split into 4 fields of comparable size, 3 in the north, one in the south, plus six smaller areas. While data analysis is still in progress, a source list of over 1000 (mostly 15 μm) sources is being published, including starburst galaxies and AGNs (type-1 and type-2), typically at z < 0.5, with several quasars (including various BAL QSOs) found up to the highest z.

9.2.3. ***The ISOCAM observations of the two Hubble Deep Fields***

Very successful programs by the Hubble Space Telescope have been the two ultradeep exposures in black fields areas, one in the North and the other in the South, called the Hubble Deep Fields (HDF). These surveys promoted a substantial effort of multi-wavelength studies aimed at characterizing the SEDs of distant and high-z galaxies. These areas, including the Flanking Fields for a total of $\sim$ 50 sq. arcmin, have been observed by ISOCAM (P.I. M. Rowan-Robinson) at 6.7 and 15 μm, achieving completness to a limiting flux of 100 μJy at 15 μm.

These have been among the most sensitive surveys of ISO and have allowed to discover luminous starburst galaxies over a wide redshift interval up to z = 1.5 (Rowan-Robinson et al. 1997; Aussel et al, 1999). In the inner 10 sq. arcmin, the exceptional images of HST provided a detail morphological information for ISO galaxies at any redshifts (see Figure 4). Furthermore, these two fields benefit by an almost complete redshift information (Cohen et al. 1999), allowing a very detailed characterization of the faint distant IR sources.

9.2.4. ***ISOCAM survey of two CFRS fields***

Two fields from the Canada-France Redshift Survey (CFRS) have been observed with ISOCAM to intermediate depths: the '14+52' field (observed at 6.7 and 15 μm) and the '03+00' field (with only 15μm data, but twice as deep). The CFRS is, with the HDFs, one of the best studied fields with multi-wavelength data. Studies of the galaxies detected in both fields have provided the first tentative interpretation of the nature of the galaxies detected in ISOCAM surveys (Flores et al. 1999).

9.2.5. ***The ISOPHOT FIRBACK survey program***

FIRBACK is a set of deep cosmological surveys in the far-IR, specifically aimed at detecting at 170 μm the sources of the far-IR background (P.I. J.L. Puget, see Puget et al. 1999). Part of this survey was carried out in the Marano area, and part in collaboration with the ELAIS team in ELAIS N1 and N2, for a total of 4 sq. degrees. This survey is limited by extragalactic source confusion in the large ISOPHOT beam (90 arcsec) to $S_{170} \geq$ 100 mJy. Some constraints on the counts below the confusion limit obtained from a fluctuation analysis of one Marano/FIRBACK field are discussed by Lagache & Puget (2000) (Sect. 9.4). The roughly 300 sources detected are presently targets of follow-up observations, especially using deep radio exposures of the same area to help reducing the large ISO errorbox and to identify the optical counterparts. Also an effort is being made to follow-up these sources with sub-mm telescopes (IRAM, SCUBA): this can provide significant constraints on the redshift of sources which would be otherwise very difficult to measure in the optical (Sect 12.2).

9.2.6. ***The Lensing Cluster Surveys***

Three lensing galaxy clusters, Abell 2390, Abell 370 and Abell 2218, have received very long integrations by ISOCAM (Altieri et al 1999). The lensing has been exploited to achieve even better sensitivities with respect to ultra-deep blank-field surveys (e.g. the HDFs), and allowed detection of sources between 30 and 100 μJy at 15 μm. However this was obviously at the expense of distorting the areal projection and ultimately making uncertain the source count estimate.

9.2.7. ***The Japanese Guaranteed Time surveys***

An ultra-deep survey of the Lockman Hole in the 7μm ISOCAM band was performed by Taniguchi et al. (1997; the survey field is different from that of the GITES Lockman survey). Another field, SSA13, was covered to a similar depth (P.I. Y. Taniguchi). The Lockman region was also surveyed with ISOPHOT by the same team: constraints on the source counts at 90 and 175 μ were derived by Matsuhara et al. (2000) based on a fluctuation analysis.

9.3. Data reduction

ISOCAM data need particular care to remove the effects of glitches induced by the frequent impacts of cosmic rays on the detectors (the 960 pixels registered on average 4.5 events/sec). This badly conspired with the need to keep them cryogenically cooled to reduce the instrumental noise, which implied a slow electron reaction time and longterm memory effects. For the deep

surveys this implied a problem to disentangle faint sources from trace signals by cosmic ray impacts.

To correct for that, tools have been developed by various groups for the two main instruments (CAM and PHOT), essentially based on identifying patterns in the time history of the response of single pixels, which are specific to either astrophysical sources (a jump above the average background flux when a source falls on the pixel) or cosmic ray glitches (transient spikes followed by a slow recovery to the nominal background). The most performant algorithm for CAM data reduction is PRETI (Stark et al. 1999), a tool exploiting multi-resolution wavelet transforms (in the 2D observable plane of the position on the detector vs. time sequence). An independent method limited to brighter flux sources, developed by Désert et al. (1999), has been found to provide consistent results with PRETI, in the flux range in common. Other methods have been used by Oliver et al. (2000a) and Lari et al. (2000). These various detection schemes and photometry algorithms have been tested by means of very sophisticated Monte Carlo simulations, including all possible artifacts introduced by the analyses.

With simulations it is has been possible to control as a function of the flux threshold: the detection reliability, the completeness, the Eddington bias and photometric accuracy ($\sim$ 10% where enough redundancy was available, as for CAM HDFs and Ultradeep surveys). Also the astrometric accuracy is good (of order of 1-2 arcsec for deep highly-redundant images), allowing straightforward identification of the sources (Aussel et al. 1999, see Fig. 4). The quality of the results for the CAM surveys is proven by the very good consistency of the counts from independent surveys (see Fig. [5] below).

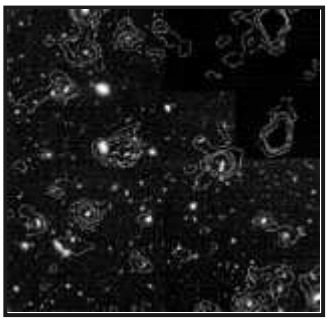

Figure 4. ISOCAM LW3 map (λ_{eff} = 15 μm, yellow contours) of the Hubble Deep Field North by Aussel et al. (1999), overimposed on the HST image. The (green) circles are the LW2 (λ_{eff} = 6.7 μm) sources. The figure illustrates the spatial accuracy of the ISO deep images with LW3, allowing a reliable identification of the IR sources [courtesy of H. Aussel].

Longer wavelength ISOPHOT observations also suffered from similar problems. The 175μm counts from PHOT C200 surveys are reliable above the confusion limit S_{170} $\sim$ 100 mJy, and required only relatively standard procedures of baseline corrections and "de-glitching". More severe are the noise problems for the C100 90μm channel, which would otherwise benefit by a better spatial resolution than C200. The C100 PHOT survey dataset is still presently under analysis.

9.4. Mid-IR and far-IR source counts from ISO surveys

IR-selected galaxies have typically red colors, because of the dust responsible for the excess IR emission. The most distant are also quite faint in the optical. For this reason the redshift information is available only for very limited subsamples (e.g. in the HDF North and CFRS areas). In this situation, the source number counts, compared with predictions based on the local luminosity function, provide important constraints on the evolution properties.

Particularly relevant information comes from the mid-IR samples selected from the CAM GITES and HDF surveys in the LW3 (12-18 μm) filter, because they include the faintest, most distant and most numerous ISO-detected sources. They are also easier to identify because of the small ISO error box for redundant sampling at these wavelengths.

Surveys of different sizes and depths are necessary to cover a wide dynamic range in flux with enough source statistics, which

justified performing a variety of independent surveys at different flux limits. The differential counts based on these data, shown in Fig. 5, reveal an impressive agreement between so many independent samples. Including ELAIS and IRAS survey data, the range in fluxes would reach four orders of magnitude. The combined 15 μm differential counts display various remarkable features (Elbaz et al. 1999): a roughly euclidean slope from the brightest IRAS observed fluxes down to $S_{15} \sim 5$ *mJy*, a sudden upturn at $S_{15} < 3$ *mJy*, with the counts increasing as $dN \propto S^{-3.1} dS$ to $S_{15} \sim 0.4$*mJy*, and evidence for a flattening below $S_{15} \sim 0.3$*mJy* (where the slope becomes quickly sub-Euclidean, $N \propto S^{-2}$).

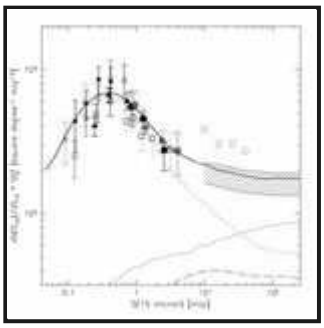

Figure 5. Differential counts at $\lambda_{eff} = 15\ \mu m$ normalized to the Euclidean law ($N[S] \propto S^{-2.5}$; the differential form is preferred here because all data points are statistically independent). The data come from an analysis of the GITES surveys by Elbaz et al. (1999). The dotted line corresponds to the expected counts for a population of non-evolving spirals. The dashed line comes from our modelled population of strongly evolving starburst galaxies, while the long-dashes are AGNs. The shaded region at $S_{15} > 10$ *mJy* comes from an extrapolation of the faint 60 μm IRAS counts by Mazzei et al. (2000).

The areal density of ISOCAM 15μm sources at the limit of $\sim$50-80 μJy is $\sim$5 arcmin^{-2}. This is nominally the ISO confusion limit at 15 μm, if we consider that the diffraction-limited size of a point-source is $\sim$ 50 arcsec^2: from eq. (8.26) and for β = -2, confusion sets in at a source areal density of 0.1/resolution element, or 7/*arcmin*^{2} in our case. The IR sky is so populated at these wavelengths that ISO was confusion limited longwards of $\lambda = 15\ \mu m$. This will also be the case for NASA's SIRTF (due to launch in mid 2002), in spite of the moderately larger primary collector (85cm).

Obviously, far-IR selected samples are even more seriously affected by confusion. The datapoints on the 175μm integral counts reported in Fig. 6 come from the FIRBACK survey. Similarly deep observations at 90, 150 and 175 μm are reported by Iuvela, Mattila & Lemke (2000). Given the moderate depth of these direct counts, background fluctuation analyses were used to constrain their continuation below the survey detection limit. The analysis of small-scale fluctuations in one FIRBACK field by Lagache & Puget (2000) produced $\sigma_{conf} \simeq 0.07$ *MJy*/*sr* with a beam of size $\omega \simeq 6\ 10^{-4}$ *sr*. From eq. [8.25], this may be used to constrain the continuation of the counts in Fig. 6 fainter than 100 mJy.

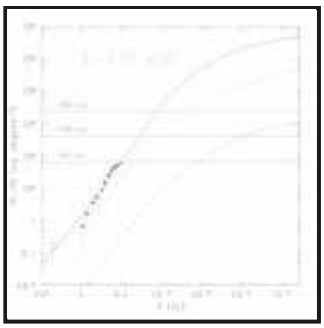

Figure 6. Integral counts based on the ISOPHOT FIRBACK survey (Sect.10.2.5) at λ_{eff} = 175 μm (filled circles, from Dole et al. 2000) nd on the ISOPHOT Serendipitous survey. The dashed and dot-dashed lines correspond to the non-evolving and the strongly evolving populations as in Fig. 5. The lowest curve is the expected (negligible) contribution of AGNs. The horizontal lines mark the confusion limits for three telescope sizes (based on eq. 8.26): the lines marked "60cm" and "360cm" correspond to the ISO and FIRST limits for faint source detection.

The 15μm counts in Fig. 5 display a remarkable convergence below $S_{15} \sim 0.2\ mJy$, proven by at least three independent surveys. The asymptotic slope flatter than -1 in integral count units implies a modest contribution to the integrated CIRB flux by sources fainter than this limit, unless a sharp upturn of the counts would happen at much fainter fluxes with very steep number count distributions, a rather unplausible situation. A meaningful estimate of the CIRB flux can then be obtained from direct integration of the observed mid-IR counts (the two datapoints at 15 and 7 μm in Fig. 3). If we further consider how close these are to the upper limits set by the observed TeV cosmic opacity (Fig. 3), the ISOCAM surveys appear to have resolved a significant (50-70%) fraction of the CIRB in the mid-IR. On the other hand, the depth of the ISO far-IR surveys (FIRBACK) is not enough to resolve more than ten percent of the CIRB at its peak wavelenth.

10. EXPLORATIONS OF THE DEEP UNIVERSE BY LARGE MILLIMETRIC TELESCOPES

Galaxy surveys in the sub-millimeter waveband offer a unique advantage for the exploration of the distant universe: the capability to naturally generate volume-limited samples from a flux-limited survey. This property is due to the peculiar shape of galaxy spectra in the sub-mm, with an extremely steep slope from 1 mm to 100 μm, as illustrated in Figure 2 for the prototype dusty starburst galaxy M82.

While above a few mm the luminosity is dominated by synchrotron and free-free radio emission, from 100 μm to 1 mm dust continuum emission dominates, with slopes as steep as $L(\nu) \propto \nu^{3.5}$ (see Sect. 3). Then, as we observe at sub-mı wavelengths galaxies at larger and larger redshifts, the rest-frame flux density moves to higher and higher frequencies along a steeply increasing spectrum, and the corresponding K-correction almost completely counter-balances the cosmic dimming of the observed flux, for a source of given luminosity at $z \geq 1$. The source flux keeps roughly constant with redshift up to $z \sim 10$, assuming cosmic sources were already present and dusty so early.

A further related advantage of sub-mm surveys is that local galaxies emit very modestly at these wavelengths. Together with the very favorable K-correction, this implies that a sensitive sub-mm survey will avoid local objects (stars and nearby galaxies) and will select preferentially sources at high and very high redshifts: a kind of direct picture of the high-redshift universe, impossible to obtain at other frequencies, where surveys are dominated by galaxies at modest redshifts if not by galactic stars. Finally, and similarly to the ISO surveys, observing in the sub-mm has the advantage of producing samples completely unaffected by

intergalactic opacity and dust extinction.

The third breakthrough event after 1996 for IR/sub-mm cosmology has come from operation of a powerful array of bolometers (SCUBA) at the focal plane of the sub-mm telescope JCMT on Mauna Kea. The success of SCUBA on JCMT was due to a combination of three crucial factors: a sensitive detector array with good multiplexing capability (37 bolometers on a field of 2 arcmin diameter, with a diffraction-limited spatial resolution of 15 arcsec), put at the focal plane of a powerful sub-mm telescope (15m dish), on a site allowing to operate at short enough wavelengths (850 μm) to exploit the very steep shape of sub-mm SED's of galaxies. For comparison, in spite of the larger collecting area, the competing bolometer array camera on the IRAM 30m telescope at Pico Veleta (Spain) is limited to work at wavelengths > 1.2 mm by the poorer, lower-altitude site, which means by itself a factor 5 penalty in the detectable source flux with respect to SCUBA/JCMT.

The latter had a long development phase (almost like a space project!), partly because of the difficulty to keep the microphonic noise within acceptable limits. But eventually, its long-sought results have come, and the instrument is providing new very exciting facts to observational cosmology.

Basically, SCUBA/JCMT has allowed to partly resolve the long- λ (850 μm) CIRB background into a population of faint distant, mostly high-z sources, as discussed in Sect. 12.3 below. During three years of activity, largely dedicated to deep surveys, SCUBA has discovered several tens of sub-millimetric sources, mostly at 850 μm.

Four main groups have used SCUBA for a variety of deep integrations. Smail et al. (1997, 1999) have undertaken an ingenious program exploiting distant galaxy clusters as cosmic lenses to amplify the flux of background sub-mm sources and to improve the spatial resolution at the source. Their sample includes now 17 sources brighter than $S_{850} = 6\ mJy$. Hughes et al. (1998) published a single very deep image of the HDF North containing 5 sources at $S_{850}(4\sigma) \geq 2\ mJy$.

Barger et al. (1998), while detecting only 2 sources down to 3 mJy, have carried out a very successful program of follow-up of SCUBA sources with optical telescopes on Mauna Kea. Eales et al. (1999) and Lilly et al. (1999) have published 12 sources to 3 mJy [a richer sample of 20 more sources is being published].

All these deep integrations are requiring many tens of hours each of especially good weather, which meant a substantial fraction of the JCMT observatory time. In spite of this effort, the surveyed areas (few tens of $arcmin^2$) and number of detected sources are quite modest, which illustrates the difficulty to work from ground at these wavelengths.

The extragalactic source counts at 850 μm, reported in Figure 7, show a dramatic departure from the Euclidean law [$N(>S) \propto S^{-2}$ in the crucial flux-density interval from 1 to 10 mJy], a clear signature of the strong evolution and high redshift of SCUBA-selected sources. Only 4 of them have been detected also at 450 μm, the sky transmission at Mauna Kea in this atmospheric channel is usually poor.

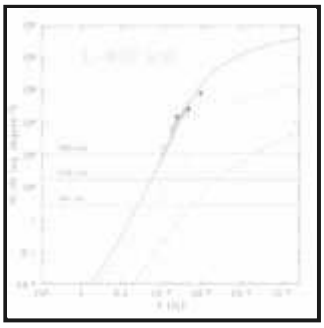

Figure 7. Integral counts at λ_{eff} = 850 μm (see also caption to Fig. 6).

More recently, a new powerful bolometer array (MAMBO) has been put in operation on IRAM. Bertoldi et al. (2000) report the first results of observations at λ_{eff} = 1.2 *mm* from a survey of 3 fields with a total area of over 300 $arcmin^2$ to a flux limit of few mJy.

11. INTERPRETATIONS OF FAINT IR/MM GALAXY COUNTS

11.1. Predictions for non-evolving source populations in the mid-IR

A zero-th order approach to interprete the deep count observations is to compare them with the expectations of models assuming no-evolution for cosmic sources. Any such calculations have to account for the effects of the very complex spectrum of galaxies in the mid-IR (including strong PAH emission and silicate absorption features, see Fig. 9) in the K-correction factor appearing in eq. (8.19), which in terms of the system transmission function $T(\lambda)$ is more appropriately written as:

$$K(L,z) = \frac{(1+z)\ \int_{\lambda_1}^{\lambda_2} d\lambda\ \left(\frac{\lambda_0}{\lambda}\right)\ T(\lambda)\ L[\nu(1+z)]}{\int_{\lambda_1}^{\lambda_2} d\lambda\ \left(\frac{\lambda_0}{\lambda}\right)\ T(\lambda)\ L[\nu, z=0]}.$$

The effect on the source flux and on the counts [eq. 8.18] may be particularly important in the wide LW3 (12-18 μm) filter. The prominent mid-IR features imply a complication when interpreting the counts, but at the same time they imply an enhanced sensitivity of the LW3 source selection to the details of the evolution of sources in the redshift interval $0.5 < z < 1.3$, which is known to be so critical for the formation of structures in the universe.

Local mid-IR luminosity functions have been published by Rush et al. (1993), Xu et al. (1998) and Fang et al. (1998) based on the 12 μm all-sky IRAS survey, see Figure 8. Unfortunately, in spite of the proximity of the CAM LW3 and IRAS 12 micron bands, at the moment we do not have a reliable LLF at 15 μm because of: a) uncertainties in the IRAS 12 μm photometry, b) the effects of local inhomogeneities, particularly the local Virgo super-cluster; and c) the flux conversion between the IRAS and CAM-LW3 bands (Elbaz et al. 1999).

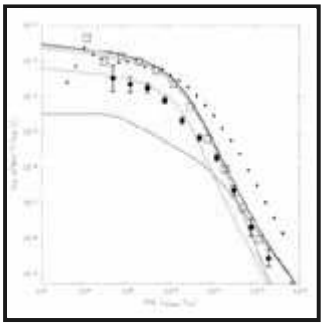

Figure 8. Galaxy LLF's at 12 μm from Xu et al. (1998 , red open squares) compared with the IRAS 60 μm LLF by Saunders et al. (1990 , small filled squares). Black ellipses are an estimate of the 12 μm LLF of active galaxies (including type-I [red line] and type-II AGNs plus starbursts [green line]) based on the (revised) catalogue by Rush et al. (1993) . Active galaxies clearly dominate the LLF at high luminosities.

The dotted line in Fig. 5 corresponds to the present best estimate of the contribution from a non-evolving population with a luminosity function consistent with that in the IRAS 12 μm band derived by Xu et al. and Fang et al. The correction to the CAM LW3 band is made assuming a 12 to 15 μm flux ratio which is a function of the 12 μm luminosity: for the less luminous objects the ratio is based on the observed mid-IR spectrum of quiescent spirals, while for the highest luminosity galaxies the ratio is the one expected for ultraluminous IR galaxies, and for intermediate objects it is close to a typical starburst spectrum like the one of M82 (see continuous line in Fig. 9). The 15 to 12 μm flux ratio increases continuously with luminosity, the flux at long-wavelength being increasingly dominated by the starburst emission.

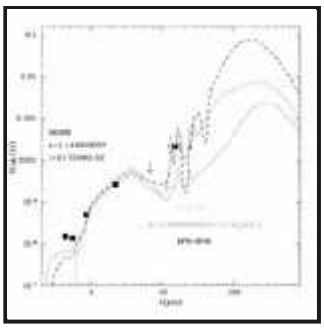

Figure 9. Broad-band spectrum of a mid-IR source selected by ISOCAM LW3 in the Hubble Deep Field North (Aussel et al. 1999), compared with the SED's of M82 (thick continuous line), Arp 220 (dashed line), and M51 (dotted line). Estimates of the SF rate [based on the M82 and Arp 220 templates] and of the stellar mass [based on the M51 template] are indicated.

It is clear that the no-evolution prediction, even taking into account the effects of the PAH features on the K-corrections, falls very short of the observed counts at fluxes fainter than a few mJy. Also the observed slope in the 0.4 to 4 mJy flux range ($N[S] \propto S^{-3\pm0.1}$) is very significantly different from the no-evolution predicted dependence $N(S) \propto S^{-2}$. The extrapolation to the bright fluxes is instead consistent, within the uncertainties, with the IRAS 12 μm counts with a slope close to Eclidean.

11.2. Evidence for a strongly evolving population of mid-IR galaxies

The shape of the differential counts shown in Fig. 5 contains relevant indications about the properties of the contributing source populations. In particular the almost flat (Euclidean) normalized counts extending from the bright IRAS fluxes down to a few mJy, followed by the sudden upturn below, suggests that is not likely the whole population of IR galaxies that evolve: in this case and for the observed IR galaxy LLF, the super-Euclidean increase in the counts would appear at brighter fluxes and not be as abrupt. This behaviour is better consistent with a locally small fraction of IR galaxies to evolve.

The IR counts in Fig. 5 are reproduced with the contribution of two source populations, one evolving, the other with constant properties as a function of time. The local fraction of the evolving starburst population is only several percent of the total, consistent with the observed fraction of interacting galaxies ($\sim$ 5% locally), the quick upturn in the counts then requiring quite a strong evolution to match the peak in the normalized counts around $S_{15} \simeq 0.5$ mJy. The details of the fit depend on the assumed values for the geometrical parameters of the universe. For a zero-Λ open universe (in our case $H_0 = 50$ *Km/sec/Mpc*, $\Omega_m = 0.3$), a physically credible solution would require a redshift increase of the comoving density of the starburs sub-population and at the same time an increase of the luminosities respectively as

$$n(L[z], z) = n_0(L_0) \times (1+z)^6 \qquad L(z) = L_0 \times (1+z)^3. \quad (11.27)$$

These are quite extreme evolution rates, if compared with those observed in optical samples for the merging and interacting galaxies (e.g. Le Fevre et al. 2000). The inclusion of a non-zero cosmological constant, and the corresponding increase of the cosmic timescale from z = 0 to 1, tend to make the best-fitting evolution rates less extreme. For $H_0 = 50$ *Km/sec/Mpc*, $\Omega_m = 0.2$, $\Omega_\Lambda = 0.8$, a best-fit to the counts requires:

$$n(L[z], z) = n_0(L_0, z) \times (1+z)^{4.5}, \qquad L(z) = L_0 \times (1+z)^2 \quad (11.28)$$

To be consistent with data on the z-distributions from the ISO source samples in the HDF (Aussel et al. 1999, 2000, see Fig. 10) and with the observed CIRB intensity, this fast evolution should turn over at $z \simeq 1$ and the IR emissivity should keep roughly

constant at higher z. An accurate probe, however, of hidden SF in the interval $1 \leq z \leq 2$ will only be possible with the longer-wavelength broad-band channel of SIRTF at $\lambda_{eff} = 24\,\mu m$.

In our scheme, *any single galaxy would be expected to spend most of its life in the quiescent (non-evolving) phase, being occasionally put by interactions in a short-lived (few 10^7 yrs) starbursting state. The evolution for the latter may simply be due to an increased probability in the past to find a galaxy in such an excited mode. Then the density evolution in eq. (11.28) scales with redshift as the rate of interactions due to a simple geometric effect following the increased source volume density. The luminosity evolution may be interpreted as an effect of the larger gas mass available to the starbursts at higher z.*

Note, however, that the above evolutionary scheme is by no means the only one able to fit the data, other solutions may be devised (e.g. the one by Xu [2000] allowing the whole local population to evolve with cosmic time).

11.3. A panchromatic view of IR galaxy evolution

Deep surveys at various IR/sub-mm wavelengths can be exploited to simultaneously constrain the evolution properties and broad-band spectra of faint IR sources. Franceschini et al. (2000) have compared the 15 μm survey data with those coming from the IRAS 60 μm, the FIRBACK 175 μm, the ELAIS 90 μm, and the SCUBA 850 μm surveys, which are the deepest, most reliable available at the moment. Information on both number counts and the source redshift distributions were used in these comparisons.

Further essential constraints, providing the local boundary conditions on the evolution histories, are given by the multi-wavelength local luminosity functions. In addition to the 12 and 15 μm LLF's, as discussed in Section 11.1, the galaxy LLF is particularly well known at 60 μm after the IRAS all-sky surveys and their extensive spectroscopic follow-up (Saunders et al. 1990). Dunne et al. (2000, see also Franceschini, Andreani, Danese 1998) attempted to constrain the galaxy LLF in the millimeter, based on *mm* observations of complete samples of IRAS 60 μm galaxies.

As previously mentioned, the properties of LLF's observed at various IR/sub-mm wavelengths can be explained only assuming that the galaxy IR SED's depend on bolometric luminosity. Fig. 8 shows that the 60μm LLF has a flatter (power-law) shape at high-L compared with the mid-IR LLF's (a fact explained in Sect. 6.6 as an effect of spectra for luminous active galaxies showing excess 60 μm emission compared to inactive galaxies [see also the L-dependence of the IRAS colours]).

Franceschini et al. (2000) have modelled in some detail the redshift-dependent multi-wavelength LLF's of galaxies by assuming for both non-evolving spirals and active starburst galaxies spectral energy distributions dependent on luminosity, with spectra ranging from those typical of inactive spirals for low-luminosities, to the 60μm-peaked spectra of luminous and ultra-luminous IR galaxies as previously described. For the SED's of intermediate luminosity objects, linear interpolations between the two as a function of bolometric luminosity were assumed. This allows to simultaneously fit the LLF's at the various wavelengths. For comparison, solutions with single spectral energy distributions for the evolving populations were also tried.

Altogether, the observed long-wavelength counts and CIRB intensity, when compared with typical galaxy SED's and the multi-wavelength LLFs, require a substantial increase of the IR volume emissivity of galaxies with redshift (see Figs. 3, 5, 7).

Should one assume that the IR SED of the ultra-luminous galaxy Arp 220 is representative of the average spectrum of the evolving population detected by ISOCAM LW3, then the consequence would be that the observed far-IR counts and the CIRB intensity are far exceeded. On the contrary, if we assume for the IR evolving sources a more typical starburst spectrum (like the one of M82, by all means similar to those of other luminous starbursts observed by ISO), then most of the observed properties of far-IR galaxy samples (number counts, redshift distributions, luminosity functions) are appropriately reproduced. Best-fits to the counts based on the M82 template are given in Figs. 6 and 7.

The good match to the multi-wavelength counts obtained by assuming a typical starburst spectrum for the evolving population already indicates that the faint IR-selected source population is likely dominated by processes of star-formation in distant galaxies more than by AGN emissions. This seems indeed the result of the first spectroscopic studies of faint ISO sources (Sect. 12.1), although a more substantial effort is required to confirm it. Considering the different shapes of the IR SEDs for SBs and AGNs, this would imply that the population detected by ISO in the mid-IR not only contributes a major fraction of CIRB at 15μ, but is also responsible for a majority contribution of the CIRB at any wavelengths.

12. NATURE OF THE FAST EVOLVING SOURCE POPULATION

12.1. Tests of the evolving IR population in the HDFs and CFRS fields

The ISO observatory has deeply surveyed with CAM LW3 some of the best investigated sky areas, in particular the two Hubble Deep Fields (North & South, Rowan-Robinson et al. 1997, Oliver et al. 2000b) and the area CFRS 1415+52 (Flores et al. 1999). Given the variety of multi-wavelength data and the almost complete spectroscopic follow-up, the surveys in these areas have allowed to achieve important tests of the evolving population responsible for the upturn of the ISO mid-IR counts and for a substantial fraction of the CIRB.

Aussel et al. (1999 and 2000) report reliably tested (see Sect. 9.3) complete samples of 49 and 63 sources to $S_{15} \geq 100 \mu Jy$ in the HDF North and South respectively, covering similar areas of 25 sq. arcmin each. Flores et al. (1999) analyse a sample of 41 sources brighter than $S_{15} \sim 300 \mu Jy$ ($S/N > 4$) over an area of 10' × 10' in CFRS 1415+52. The vast majority (90%) of the ISO sources in the HDF surveys have spectroscopic redshifts, and for the remaining objects photometric redshifts are easily estimated. The redshift distributions $d(z)$ for the HDF and CFR1415 surveys are reported in Figure 10, and compared with the model fitting the multi-wavelength counts mentioned in Sect. 11.2. Although the two surveys cover individually small sky areas, the fair match between them gives some confidence about the overall reliability of the result. These data set a stringent limit on the rate of cosmological evolution for IR galaxies above $z \sim 1$, which needs to level off to avoid exceeding the observed $d(z)$ on the high-z tail. Note however that the observed high-z convergence of $d(z)$ is also partly an effect of the strong K-correction in the LW3 flux for dust-rich galaxies (see an example in Fig. 9): disentangling K- from evolutionary-corrections at $z > 1$ will require SIRTF and FIRST.

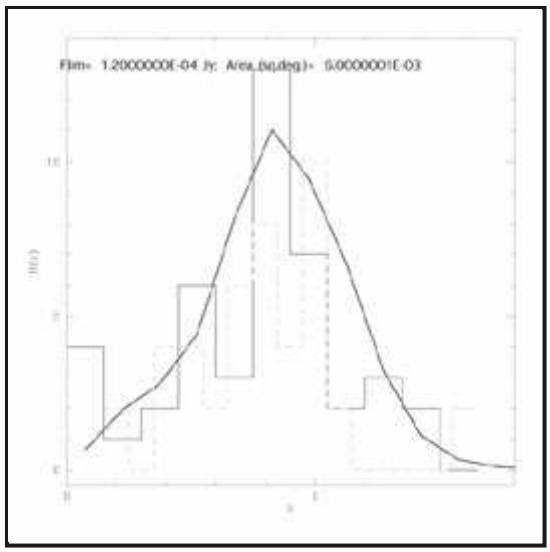

Figure 10. Redshift distributions from the HDFN (Aussel et al. 2000) and CFRS 1415+52 ISOCAM LW3 samples, compared with model predictions.

HST imaging data on these fields provide detailed morphological information on ISO sources. Elbaz et al. (1999) and Aussel et al. (1999) find that 30 to 50% of them show clear evidence of peculiarities and multiple structures, in keeping with the local evidence that galaxy interactions are the primary trigger of luminous IR starbursts. From their Caltech redshift survey in the HDF North, Cohen et al. (1999) report that over 90% of the faint LW3 ISO sources are members of galaxy concentrations and groups, which they identify as peaks in their redshift distributions. Indeed, it is in these dense galaxy environments with low velocity dispersion that interactions produce resonant perturbation effects on galaxy dynamics.

12.1.1. *Optical and NIR spectral properties: nature of the IR sources*

Flores et al. (1999) report a preliminary analysis of the spectra of IR sources in CFRS 1415+52, noting that a majority fraction of these display both weak emission (OII 3787) and absorption (H_δ) lines, as typical of the *e(a)* galaxy spectral class: the latter is mentioned in the literature as a post-starbursting population, one in which a vast population of A-type absorption-line stars from a $\sim$ 1 Gyr old massive starburst combine with a small residual of ongoing SF evidenciated by the weak OII emission. Given the far-IR selection of the faint ISO sources, which is expected to preferentially detect dusty star-forming galaxies, this result would be difficult to understand, as it lets open the question of "why the ongoing active starbursts are not detected".

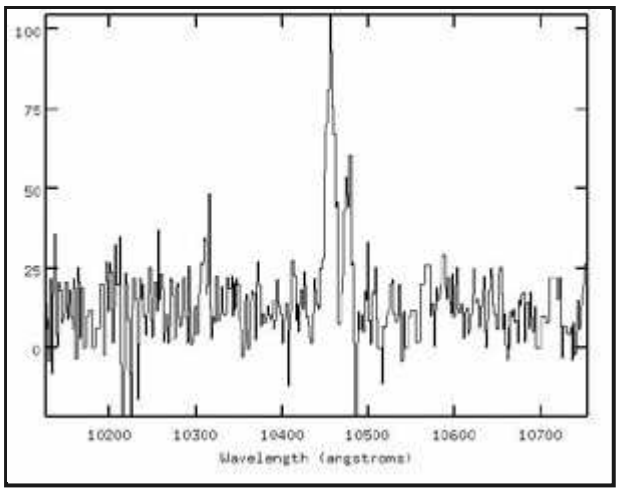

Figure 11. ISAAC/VLT spectrum of HDFS source # 53 at z = 0.58. The $H\alpha$ and NII redshifted lines are clearly visible [from Rigopoulou et al. 2000].

Rigopoulou et al. (2000) and Franceschini et al. (2000b) have observed with ISAAC on VLT a sample of 13 high-z ($0.2 < z < 1.4$) galaxies selected in the HDF South to $S_{15} > 100\ \mu Jy$: *the $H\alpha$ line is detected in virtually all of the sources, and found quite prominent (EW > 50 Å), indicating substantial rates of SF after de-reddening corrections, and demonstrating that these optically faint but IR luminous sources are indeed powered by an ongoing massive dusty starburst.*

The *e(a)* spectral appearence is interpreted by Poggianti & Wu (2000) and Poggianti, Bressan, Franceschini (2000) as due to selective dust attenuation, extinguishing more the newly-formed stars than the older ones which have already disrupted their parent molecular cloud.

These papers independently found that $\sim$ 70 - 80% of the energy emitted by young stars and re-processed in the far-IR leaves no traces in the optical spectrum, hence can only be accounted for with long-wavelength observations.

12.1.2. Evaluating baryonic masses and the SFR of the IR population

Further efforts of optical-NIR spectroscopic follow-up of faint IR sources are planned for the next years, including attempts to address the source kinematics and dynamics based on line studies with the next-generation of IR spectrographs (e.g. SINFONI on VLT). The latter would be particularly relevant in consideration of the typically complex dynamical structure of luminous IR starbursts. At the moment, for an evaluation of the main properties of the IR population we have to rely on indirect estimates exploiting the near-IR and far-IR fluxes. One important parameter is the baryonic mass in stars, for measure of which fits of local template SEDs to the near-IR broad-band spectrum can be used. Our estimated values of the baryonic mass ($\sim 10^{11}\ M_{\odot}$,

with 1 dex typical spread, see Figure 12) indicate that already evolved and massive galaxies host the powerful starbursts.

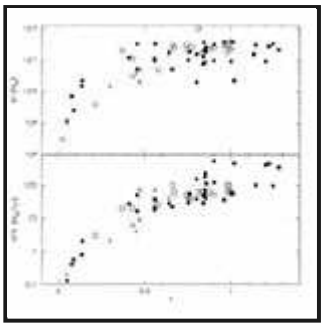

Figure 12. Star formation rates and baryonic masses as a function of redshift for galaxies selected by ISOCAM LW3 at 15 μ *m* in the HDFN and CFRS 1415+52.

As a measure of the rate of star-formation (SFR), the other fundamental parameter describing the physical and evolutionary status of the sources, we have exploited the mid-IR flux as an alternative to the (heavily extinguished) optical emissions, since it is much more directly related to the bolometric (mostly far-IR) flux, which is the most robust indicator of the number of massive reddened newly-formed stars. Vigroux et al. (1998) find that the ISOCAM mid-IR fluxes (from both LW3 and LW2 ISOCAM observations) are tightly and linearly related with the bolometric emission in local galaxies, evidence contradicted only in very extinguished peculiar sources (e.g. Arp 220), for which the mid-IR spectrum is self-absorbed. Using several HDF North sources having both the mid-IR and radio flux, Aussel et al. (2000) find that the two SFR estimators, both largely unaffected by dust extinction, provide consistent results on the SFR. However, the mid-IR flux has the advantage over the radio to be less affected by AGN emission, providing a more reliable SF measurer (Cohen et al. 1999; Aussel et al. 2000; Franceschini et al. 2000b). Also the fact that only 7 of the 49 IR SBs in the HDFN are detected in radio to a flux limit of few tens of μJy tells that the mid-IR flux is a more sensitive indicator of SF. This untill dedicated space missions (in particular the 3.6m FIRST observatory) will measure the peak of dust emission at $\lambda \sim 100\,\mu m$ in high-redshift galaxies with high accuracy.

Altogether, the galaxy population dominating the faint mid-IR counts and substantially contributing to the bolometric CIRB intensity (assumed typical SB SEDs) appears to be composed of luminous ($L_{\rm bol} \sim 10^{11}$ - $10^{12}\,L_{\odot}$) starbursts in massive ($M \sim 10^{11}\,M_{\odot}$) galaxies at $z \sim 0.5$ - 1, observed during a phase of active stellar formation. The typically red colors of these systems suggest that they are mostly unrelated to the faint blue galaxy population dominating the optical counts (Ellis 1997), and should be considered as an independent manifestation of (optically hidden) star formation (Elbaz 1999; Aussel 1998).

12.2. What are the FIRBACK 175 μm sources?

The nature of the 175 μm sources discovered by FIRBACK/ISO, and contributing $\sim$ 10% of the CIRB intensity, is presently the target of intense observational and modellistic investigations, although no conclusions are possible at the moment. Because of the missing knowledge of the LLF, the interpretation of the 175μm counts themselves is subject to some uncertainties: is there strong or marginal evidence for evolution at the survey limit of 100 mJy (Fig. 6)? Dole et al. (2000) argue in favour of the former, while Fig. 6 reports a solution in which a moderate-redshift ($z \sim 0.5$) population still dominates there.

The basic limitation comes from the difficulty to identify the optical counterparts, due to the large (40 arcsec) ISOPHOT error-box. Progress is being achieved by cross-correlating with deep radio surveys available in the FIRBACK fields (exploiting the good radio/FIR correlation, eq. 6.14) and by means of some limited SCUBA follow-up. Scott et al. (2000) have obtained data at 450 and 850 μm for 10 FIRBACK sources: the FIR-mm SEDs tentatively indicate, for plausible far-IR spectra, redshifts in the range from 0 to 0.4 for the majority of the sources, while a few may be at $z > 1$.

Mid-IR 15 μm fluxes from an ISOCAM map are available in the *"FIRBACK Marano"* area, which indicate that the 15μm counterparts of the 175μm sources are rather faint (Elbaz, 1999). Three interpretations have been suggested: (a) FIRBACK sources are typically very high-luminosity Arp220-like at low redshift ($z \sim 0.1$-0.4); (b) they are more standard starbursts at $z > 1$; (c) they are low-activity spirals at moderate z with significant amounts of cold-dust and excess emission at $\lambda > 100\mu m$.

Although the results of the SCUBA observations might indicate that the last interpretation could be more probable, the nature of the FIRBACK source population is far from proven, further multi-wavelength data being required to address it. Deeper far-IR observations will be possible with SIRTF, but a more final solution will probably require the FIRST's better spatial resolution.

12.3. The nature of the high-z galaxies detected in the millimeter

Thanks to the unique advantage for deep sub-mm observations offered by the very peculiar K-correction, sub-mm surveys with sensitivities of few mJy at 850μm, have been able to detect high-redshift (very luminous) sources in flux-limited samples. The observed 850 μm counts, far in excess of the no-evolution prediction, already tell incontrovertibly about the cosmological distance and evolutionary status of the SCUBA-selected source population.

Unfortunately, probing directly the nature of these objects via optical identification and spectroscopic follow-up turned out to be very difficult, in spite of the substantial efforts dedicated. The SCUBA diffraction-limited HPBW at 850 μm is large, $\sim$ 15 arcsec FWHM, and the difficulty of the identification is further exacerbated by the usual extreme faintness of the optical counterparts, as demonstrated in the (few) cases in which the identification has been possible (see e.g. Figure 13).

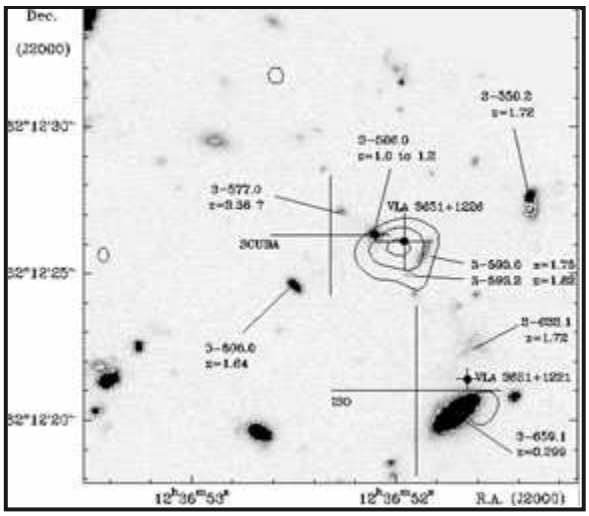

Figure 13. Map of the 1.3 mm continuum obtained with the IRAM interferometer in the field of the source HDF 850.1 by Downes et al. (1999). HDF 850.1 is the brightest source discovered at 850 μm by SCUBA (Hughes et al. 1998), and has a flux density of 2.2 mJy at 1.3 mm. The field center coincides with the center position of the SCUBA error-box, whose size is however comparable to the whole image area. The colour image is a composite of BVI data from HDF. Positions of VLA and ISO sources, as well as photometric redshift data, are also indicated. IRAM and VLA position clearly point to a faint optical counterpart of HDF 850.1 (3-593.0), possibly influenced by gravitational lensing by the elliptical 3-586.0, in a similar configuration to the prototypical primeval galaxy IRAS F10214 [courtesy of D. Downes].

The reliability of the identification has been evaluated by computing the probability that the nearest member of a population of candidate identifications with surface density n falls by chance within a distance d from the SCUBA source: $P = e^{-\pi n d^2}$. For a sample of size N of SCUBA detections, the product NP gives the number of spurious identifications (Lilly et al. 1999). This analysis has shown that the situation is not quite comfortable for the SCUBA surveys, essentially because of the faintness of the optical counterparts: roughly 50% of all identifications may be spurious.

Two approaches have been followed to improve the identification and try to characterize the population. One was to systematically survey spectroscopically all optical sources falling in the SCUBA beam, the other was to exploit cross-identifications with ultra-deep radio catalogues. Particularly well studied are the fields in the Cluster Lens Survey (Smail et al. 1997), exploiting the flux-amplification by massive foreground galaxy clusters. The current situation about redshift measurements in this survey is: the 16 SCUBA sources have 24 possible counterparts with spectroscopic redshifts, 6 reliable z estimates (a $z = 2.8$ combined AGN/starburst, a $z = 2.6$ galaxy pair, 2 galaxies with AGN signatures at $z = 1.16$ and $z = 1.06$, and finally 2 foreground cD cluster members [Barger et al. 1999]). Note that the identification with the galaxy pair has been later confirmed by CO mm observations (Frayer et al. 1999).

An interesting case is illustrated in Fig. 13, showing the brightest object HDF-850.1 in the Hughes et al. (1998) survey, confirmed by IRAM interferometry as a probable ultra-luminous lensed starburst with $L_{\rm bol} \sim 2\ 10^{12} L_{\odot}$ at $z_{\rm photom} \simeq 1.7$

The difficulty of the identification process is illustrated by the recent finding (Smail et al. 1999) of the presence of two Extremely Red Objects (ERO's) as probable counterparts of two SCUBA sources. Given the faintness of optical counterparts and the extreme difficulty to get the redshift from optical spectroscopy, some millimetric estimators of the redshift have been devised to override optical measurements. Hughes et al. (1998) use the S_{450} / S_{850} flux ratio as a measure of z. However, given the rather wide temperature-distribution of cosmic dust (see e.g. the three quite different spectral templates, for Arp 220, M82, and M51 in Fig. 9), this test proved to be very uncertain. Much more reliable the technique proposed by Carilli & Youn (1999)

to exploit the $S_{850\ \mu}/S_{20\mathrm{cm}}$ flux ratio, which has the advantage to rely on very robust mm spectral shapes at 850 μ ($S_\nu \propto \nu^{3.5}$, see Sect. 3) and in the radio (typical power-law synchrotron spectra), with opposing spectral slopes. Assuming an Arp 220 spectral template they got:

$$S_{850\mu}/S_{20cm} = 1.1 \times (1+z)^{3.8}$$

whose small scatter mostly reflects the tight FIR to radio correlation.

Population constraints on the z-distributions have been derived in this way, and the basic result (still tentative and requiring confirmation) is that *faint SCUBA sources are mostly ultra-luminous galaxies at typical* $z \sim$ *1 to* $\sim$ *3* (e.g. Barger et al. 1999). Clearly, the details of the z-distribution cannot yet be quantified with precision, this will likely require new instrumentation (mm interferometers - e.g. ALMA - are particulalry needed, in addition to space FIR observatories).

As suggested by many authors, the similarity in properties between this high-z population and local ultra-luminous IR galaxies argues in favour of the idea that these represent the long-sought "primeval galaxies", those in particular originating the local massive elliptical and S0 galaxies. This is also supported by estimates of the volume density of these objects in the field $\sim$ 2 - 4 $\times 10^{-4}$ Mpc^{-3}, high enough to allow most of the field E/S0 to be formed in this way (Lilly et al. 1999). As for the E/S0 galaxies in clusters, a very interesting result was the recent discovery by SCUBA of a significant excess of very luminous ($L \sim 10^{13} L_\odot$) sources at 850 μm close to the z = 3.8 radiogalaxy 4C41.17 (Ivison et al. 2000), which parallels the evidence of a similar excess of EROs and Lyman-break galaxies in this area. It is tentalizing to interprete these data as indicative of the presence of a forming cluster surrounding the radiogalaxy, where the SCUBA sources would represent the very luminous ongoing starbursts.

By continuity, the less extreme starbursts ($L \sim 10^{11}$ - 10^{12} $L_\odot$) discovered by ISOCAM at lower redshifts can possibly originate the spheroidal components in later morphological type galaxies (see more in Sect. 13.2.4 below).

12.4. AGN contribution to the energetics of the faint IR sources

Within this interpretative scheme, a margin of uncertainty still exists about the possible contribution by gravitational accretion from a nuclear quasar to the energy budget in these high-z IR-mm sources. While stellar energy production provides a modest overall efficiency for baryon transformations of quite less than a percent at most, the theory of gravitational accretion predicts values in the range $\epsilon \sim$ 5 - 40%. A natural question then arises as of how much of the bolometric flux in these sources is contributed by an AGN. Unfortunately, the optical-UV-soft-X ray primary source spectrum in the high-redshift IR-mm sources is almost completely re-processed by dust into an IR spectrum largely insensitive to the properties of the primary incident one.

As for SCUBA sources, there have been indications for AGN activity for at least a fraction (20-30%) of them. Indeed, since SCUBA selects the top luminosity end of the IR population, and considering the local evidence of a larger incidence of AGNs among ULIRGs, an important AGN contribution to the SCUBA sources would be expected (potentially biasing our conclusions about their contribution to the SFR history). Risaliti et al. (2000) and Bassani et al. (2000) claim evidence for a significant AGN contribution in the large majority (> 60%) of the local ULIRGs based on hard X-ray data, something confirmed also by high spatial resolution IR imaging by Soifer et al. (2000).

Since its launch the last year, the CHANDRA X-ray observatory (the ultimate imager in hard X-rays) has allowed to probe very deeply into the nature of the high-z SCUBA sources, using the hard X-ray flux as diagnostic tool (SB are weaker X-ray emitters than any kind of AGNs). Among several tens of hard X-ray and 850 μm sources detected in various independent survey areas, (Fabian et al. 2000, Hornschemeier et al. 2000, Barger et al. 2000), only very few are in common, the two samples being essentially orthogonal. Unless all these are Compton-thick and any hard X-ray scattered photons are also photoelectrically absorbed, the conclusion is that the bulk of the emission by high-luminosity SCUBA sources is due to star formation (in agreement with a dominant stellar emission in local ULIRGs found by Genzel et al. 1998).

While the detailed interplay between starburst and AGN is still an open issue even for local sources, the estimated fraction of the CIRB at 850 μm due to AGNs is not larger than 10% (Barger et al. 2000). Preliminary results of spectroscopic studies of the H_α line properties in faint ISO mid-IR sources (D. Rigopoulou, private communication) seem also to indicate a modest incidence of AGN, which would imply that the overall AGN contribution to the bolometric CIRB is likely around 10% or so.

12.5. Discussion

ISO and SCUBA surveys have proven nicely complementary capabilities to explore, within the limitations of the current instrumentation, long-wavelength emission by galaxies over most of the Hubble time, up to z of several. Unfortunately, this has been possible only at the short- and long-wavelength tails of the CIRB background spectrum: a bad coincidence makes the wavelength interval including peak emission by distant dusty galaxies ($\lambda \sim 30$ to $300\,\mu m$) hardly accessible at present.

All mentioned exploratory surveys of the distant universe have indicated that the overall volume emissivity of galaxies at long wavelengths drastically increases as a function of redshift, to explain the very steep observed multi-wavelength counts and the redshift distributions showing substantial high-z tails. This evolution, however, should level off by $z \sim 1$ (see Fig. 14 below) to allow consistency with the observed z-distributions (Franceschini et al. 2000) and the CIRB spectral shape.

A spectacular finding by the deep SCUBA surveys was the discovery of ultra-luminous galaxies at high-redshifts, mostly emitting in the far-IR and possibly at the origin of present-day galaxy spheroids. However, the most precise quantification of the cosmic history of the IR population comes at the moment from the ISO deep and ultra-deep surveys, which provide very detailed constraints on the counts (Fig. 5) and also allow to unambiguously identify in the optical the faint IR sources (Fig. 4). The outcome of our spectroscopic observations is that the faint population making up the CIRB in the mid-IR is dominated by actively star-forming galaxies with substantial $H\,\alpha$ emission (Sect. 12.1.1). Preliminary inspection of $H\,\alpha$ line profiles and constraints set by the 15 to 7 micron flux ratio indicate that the majority of sources are powered by a SB rather than an AGN.

Mid-IR ISO counts and the redshift distributions of the sources require extremely high rates of evolution of the $15\mu m$ luminosity function up to $z \sim 1$. Taking into account all effects due to the detector spectral response function to the complex mid-IR spectral features, the observable statistics may be explained in terms of a strong evolution for a population of IR starbursts contributing little to the local LF. Consequently, a plausible evolution pattern should involve both the source luminosities and spatial densities.

A natural way to account for this very high dependence on redshift of the IR starburst population is to assume that it consists of otherwise normal galaxies, but observed during a dust-extinguished luminous starburst phase, and that its extreme evolution is due to *an increased probability with z to observe a galaxy during a starburst event.*

The common wisdom that SBs are triggered by interactions and merging suggest that the inferred strong number density evolution may be interpreted as an increased probability of interaction with z. Assuming that the phenomenon is dominated by interactions in the field and a velocity field constant with z, than this probability would scale roughly as $\propto n(z)^2 \propto (1+z)^6$, n being the number density in the proper (physical) volume. A more complex situation is likely to occur, as the velocity field evolves with z in realistic cosmological scenarios and if we consider that the most favourable environment for interactions are galaxy groups, which indeed are observed to include the majority of ISOCAM distant sources (Cohen et al. 1999). The increased luminosity with z of the typical starburst is due, qualitatively, to the larger amount of gas available in the past to make stars.

To note is that closed or zero- Λ world models require evolution rates quite in excess of those inferred from deep optical imaging (Le Fevre et al. 2000), whereas our best-fit solution for $\Omega_\Lambda = 0.8$ and $\Omega_m = 0.2$ (eq. 11.28]) is closer to the optical results.

How this picture of a 2-phase evolution of faint IR sources compares with results of optical and near-IR deep galaxy surveys is matter of debate. Since, because of dust, most of the bolometric emission during a starburst comes out in the far-IR, we would not expect the optical surveys to see much of this violent IR starbursting phase. Indeed, B-band counts of galaxies and spectroscopic surveys are interpreted in terms of number-density evolution, consequence of merging, and essentially no evolution in luminosity. The Faint Blue Object population found in optical surveys may be interpreted as the "post-starburst" population, objects either observed mostly after the major event of SF, or more likely ones in which the moderately extinguished intermediate age ($\sim 10^7\ yrs$) stars in a prolonged starburst (several $10^7\ yrs$) dominate the optical spectrum. In this sense optical and far-IR selections trace different phases of the evolution of galaxies, and provide independent sampling of the cosmic star formation.

A lively debate is currently taking place about the capabilities of UV-optical observations to map accurately by themselves the past and present star-formation, based on suitable corrections for dust extinction in distant galaxies. Adelberger et al. (2000) suggest that the observed 850 μm galaxy counts and the background could possibly be explained with the optical Lyman drop-out high-z population by applying a proportionality correction to the optical flux and by taking into account the locally observed distribution of mm-to-optical flux ratios.

On the other hand, a variety of facts indicate that optically-selected and IR/mm-selected faint high-redshift sources form almost completely disjoint samples. Chapman et al. (2000) observed with SCUBA a subset of z = 3 Lyman-break galaxies having the highest estimeted rates of SF as inferred from the optical spectrum, but detected only one object out of ten. For this single detected source the predicted SFR based on the extinction-corrected optical spectrum was 5 times lower than found by SCUBA. A similar behaviour is also shared by local luminous IR galaxies, whose bolometric flux is unrelated to the optical spectrum (Sanders & Mirabel 1996).

Finally, our previously mentioned observational results by Rigopoulou et al. (2000) and the theoretical ones by Poggianti & Wu (2000) and Poggianti et al. (2001) report *independent evidence from both local and high-z luminous starbursts that typically 70% to 80% of the bolometric flux from young stars leaves no traces in the UV-optical spectrum, because it is completely obscured by dust*. As there seems to be no "a priory" way to correct for this missing energy, we conclude that only long-wavelength observations, with the appropriate instrumentation, can eventually *measure* SF in galaxies at any redshifts.

13. GLOBAL PROPERTIES: THE SFR DENSITY AND CONTRIBUTIONS TO THE CIRB

13.1. Evolution of the comoving luminosity density and SFR

As illustrated in Fig. 3, the CIRB intensity and spectral distribution are in clear support of models for evolving starbursts discussed above.

Unfortunately, we are not yet in the position to derive an independent assessment of the evolutionary SFR density based on the available complete samples of faint IR sources: although a substantial effort to follow them up in the optical has started (particularly good chances are offered by ongoing spectroscopic follow-up of the statistically rich faint ISOCAM samples like the GITES and HDFs), the process is far from complete. As a consequence, no detailed conclusions can yet be drawn about the contribution of IR sources to the global comoving luminosity and SFR densities (Madau et al. 1996).

Only rather model-dependent estimates are possible at the moment, based for example on the evolution scheme described in Sect. 11 and whose predictions are summarized in Figure 14. There is a clear indication here that the contribution of IR-selected sources to the luminosity density at high-z should significantly exceed those based on optically selected sources, and that the excess may be progressive with redshift up to $z \sim 1$.

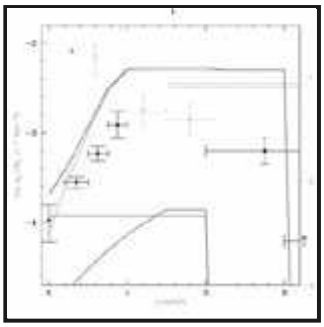

Figure 14. Evolution of the metal production rates (left axis) and of the star formation rates (right axis) based on the modelisation of IR counts and z-distributions in Sect 11.1 (case $\Omega_m = 0.3$, $\Omega_\Lambda = 0$). Data points come from optical observations. Very premilinary evaluations based on SCUBA results indicate values of the comoving densities close to or even higher than the horizontal line from z = 1 to 3 (Smail et al. 1999). The shaded horizontal line is an evaluation of the average SFR in spheroidal galaxies by Mushotzky & Loewenstein (1997).

This evolution should however level off at higher z, to allow consistency with the observed z-distributions for faint ISOCAM sources (Franceschini et al. 2000) and with the estimates of the average time-dependent emissivity $j_{\rm eff}(z)$ (eq. [8.21]) based on deconvolution of the CIRB spectrum (Gispert et al. 2000).

Altogether *these results indicate that the history of galaxy long-wavelength emission does probably follow a path similar to that revealed by optical-UV observations, by showing a similar peak activity around* $z \sim 1$*, rather than being confined to the very high-z,* as sometimes was suggested. This confirms that the bulk of the galaxy activity, and particularly the bulk of the energy released in the CIRB background, is to be placed around $z = 1$, which is obvious from Fig. 14 if the dependence of the cosmological timescale on redshift is considered (Harwit 1999; Haarsma & Partridge 1998).

These results can only be preliminary untill we will have more substantial identifications of existing IR-selected source samples, or, better, after the fleet of IR/mm facilities planned for this and the next decade will have eventually provided data of enough quality to allow a full long-wavelength complement to the optical-UV high-z observations.

13.2. Energy constraints from background observations

In the present situation, the most robust constraints on the high-redshift far-IR/sub-mm population come from observations of the global energetics residing in the CIRB and optical background radiations. The latter imply a very substantal demand on contributing sources, as detailed below in schematic terms.

Let us assume that a fraction f_* of the universal mass density in baryons

$$\rho_b = \frac{3H_0^2(1+z)^3}{8\pi G}\Omega_b \simeq 7\ 10^{10}(1+z)^3\left(\frac{H_0}{50\ Km/s/Mpc}\right)^2 \Omega_b\ [M_\odot/Mpc^3] \quad (13.29)$$

undergoes a transformation (either processed in stars or by gravitational fields) with radiative efficiency ϵ, then the locally observed energy density of the remnant photons is

$$\rho_\gamma = \rho_b \frac{c^2\epsilon f_*}{(1+z)^4} \simeq 5\ 10^{-30}\left(\frac{H_0}{50\ Km/s/Mpc}\right)^2 \frac{\Omega_b}{0.05}\frac{f_*}{0.1}\frac{2.5}{(1+z_*)}\frac{\epsilon}{0.001}[gr/cm^3]. \quad (13.30)$$

For stellar processes, ϵ is essentially determined, within the moderate uncertainties of stellar models, by the IMF: $\epsilon = 0.001$ for a Salpeter IMF and a low-mass cutoff $M_{\rm min} = 0.1\ M_\odot$ (see eq. 4.13), $\epsilon = 0.002$ and $\epsilon = 0.003$ for $M_{\rm min} = 2$ and $M_{\rm min} = 3$,

while ϵ gets the usually quoted value of $\epsilon = 0.007$ only for $M_{\rm min} > 10\ M_\odot$ [A. Bressan, private communication].

Note how the contribution to the photon background energy by very high redshifts is penalized in eq. (13.30) by the $(1 + z)^{-1}$ factor: measurements of the photon background preferentially constrain source emission at moderate z, whereas estimates of the local average metal abundance (obviously much more difficult and indirect!) would in principle provide a less biased integral over the total stellar yield in the past.

13.2.1. ***Constraints from the integrated optical background***

As already noticed (Sect. 8.3.1), the converging galaxy counts at faint magnitudes observed in the optical and near-IR allow to estimate with fair accuracy the total diffuse flux at these wavelengths (Fig. 3, see Madau & Pozzetti 2000). The bolometric emission from 0.1 to 7 μm by distant galaxies turns out to be

$$\nu I(\nu)|_{opt} \simeq (17 \pm 3)\ 10^{-9}\ Watt/m^2/sr, \quad (13.31)$$

which in fact is a lower limit if we give credit to claims of a (× 2 - 3) larger optical/NIR background, see Sect. 8.1 (but see also a counter-argument in Sect. 8.2).

We discussed evidence that for the most luminous starbursts the optical spectra are only moderately contributed by starburst

emission, which is mostly hidden in the far-IR. Accordingly, let us assume that the optical/NIR BKG mostly originates by quiescent SF in spiral disks and by intermediate and low-mass stars. As observed in the Solar Neighborhood, a good approximation to the IMF in such relatively quiescent environments is the Salpeter law with standard low-mass cutoff, corresponding to a mass-energy conversion efficiency $\epsilon \sim 0.001$. With these parameter values, we can reproduce the whole optical BKG intensity of eq. (13.31) by transforming a fraction $f_* \simeq 10\%$ of all nucleosynthetic baryons into low-mass stars, assumed the bulk of this process happened at $z_* \sim 1.5$ and 5% of the closure value in baryons (for our adopted $H_0 = 50$ *Km/s/Mpc*, or $\Omega_b h^2 = 0.012$, consistent with the theory of primordial nucleosynthesis):

$$\nu I(\nu)|_{opt} \simeq 20\ 10^{-9} \left(\frac{H_0}{50\ Km/s/Mpc}\right)^2 \frac{\Omega_b}{0.05} \frac{f_*}{0.1} \left(\frac{2.5}{1+z_*}\right) \frac{\epsilon}{0.001}\ Watt/m^2/sr.$$

It is generated in this way a local density in low-mass stars consistent with the observations (based on photometric surveys, Ellis et al. 1996, and assuming standard mass to light ratios):

$$\rho_b(stars) \simeq 7\ 10^{10} f_* \Omega_b \simeq 3.4\ 10^8\ M_\odot/Mpc^3, \quad (13.32)$$

which, assuming typical solar metallicities, corresponds to a local density in metals of

$$\rho_Z(stars) \simeq 1.6\ 10^9 f_* \frac{Z}{Z_\odot} \Omega_b\ M_\odot/Mpc^3 \simeq 7.7\ 10^6 M_\odot/Mpc^3. \quad (13.33)$$

Note that a factor 2-3 larger optical/NIR background than in eq. (13.31) could still be consistent with the present scheme if a similar scaling factor would also apply to eqs. (13.32) and (13.33): that is, if both the excess background and low-mass stars and stellar metals would be due to extended low-brightness halos, unaccounted for by deep HST imaging as well as by local photometric surveys.

13.2.2. ***Explaining the CIRB background***

The total energy density between 7 and 1000 μm contained in the CIRB, including modellistic extrapolations as in Fig. 3 consistent with the constraints set by the cosmic opacity observations, amounts to

$$\nu I(\nu)|_{FIR} \simeq 40\ 10^{-9}\ Watt/m^2/sr. \quad (13.34)$$

Following our previous assumption that luminous starbursting galaxies emit negligible energy in the optical-UV and most of it in the far-IR, we coherently assume that the energy resident in the CIRB background originates from star-forming galaxies at median $z_* \simeq 1.5$. The amount of baryons processed in this phase and the conversion efficiency ϵ have to account for the combined constraint set by eqs. (13.32) and (13.34), that is to provide a huge amount of energy with essentially no much stellar remnant in the local populations. The only plausible solution is then to change the assumptions about the stellar IMF characterizing the starburst phase, for example to a Salpeter distribution cutoff below $M_{\rm min} = 2\ M_\odot$, with a correspondingly higher efficiency $\epsilon = 0.002$ (see discussion in Sect. 13.2). This may explain the energy density in the CIRB:

$$\nu I(\nu)|_{FIR} \simeq 40\ 10^{-9} \left(\frac{H_0}{50\ Km/s/Mpc}\right)^2 \frac{\Omega_b}{0.05} \frac{f_*}{0.1} \left(\frac{2.5}{1+z_*}\right) \frac{\epsilon}{0.002}\ Watt/m^2/sr,$$

assumed that a similar amount of baryons, $f_* \simeq 10\%$, as processed with low efficiency during the "inactive" secular evolution, are processed with higher efficiency during the starbursting phases, producing a two times larger amount of metals: $\rho(metals) \sim 1.4\ 10^7\ M_\odot/Mpc^3$. Note that by decreasing $M_{\rm min}$ during the SB phase would decrease the efficiency ϵ and increase the amount of processed baryons f_*, hence would bring to exceed the locally observed mass in stellar remnants (eq. [13.32]).

The above scheme is made intentionally extreme, to illustrate the point. The reality is obviously more complex than this, e.g. by including a flattening at low mass values in the Salpeter law (see Zoccali et al 2000) for the solar-neighborhood SF and, likewise, a more gentle convergence of the starburst IMF than a simple low-mass cutoff.

13.2.3. ***Galactic winds and metal pollution of the inter-cluster medium***

A direct prediction of our scheme above is that most of the metals produced during the starburst phase have to be removed by the galaxies to avoid largely exceeding the locally observed metals in galaxies. As discussed in Sect. 6.4, there is clear evidence in local starbursts, based on optical and X-ray observations, for large-scale super-winds out-gassing high-temperature enriched plasmas from the galaxy. Our expectation would be that a substantial amount of metals, those originating from the same SF processes producing the CIRB background, are hidden in the hot inter-cluster medium.

But where all these metals are?

While densities and temperatures of the polluted plasmas in the diffuse (mostly primordial and un-processed) inter-cluster medium are such to hide easily these products of the ancient SB phase, an interesting support to the above scheme comes from consideration of the metal-enriched intra-cluster plasma (ICP) in clusters of galaxies. Rich clusters are considered to constitute a representative sample of the universe, while at the same time - given their deep gravitational potential - they are to be considered from a chemical point of view as closed boxes (all metals produced by cluster galaxies are kept inside the cluster itself).

The mass of metals in the ICP plasma is easily evaluated from the total amount of ICP baryons (measured to be $\sim$5 times larger than the mass in galactic stars) and from their average metallicity, $\sim$40% solar. The mass of ICP metals is $M_{\rm metals,\ ICP} \simeq 5 \times 0.4\ (Z/Z_{\odot})\ M_{\rm stars}$, which is two times larger than the mass of the metals present in galactic stars and consistent with the mass in metals produced during the SB phase.

Then the same starbursts producing the ICP metals are also likely responsible for the origin of the CIRB. As mentioned, the starburst enrichment process could have been pictured in a deep SCUBA image of the candidate proto-cluster surrounding the z = 3.8 radio-galaxy 4C41.17. In a similar fashion, Mushotzky & Loewenstein (1997) used their metallicity measurements in clusters to estimate the contribution of spheroidal galaxies to the SFR density (see Fig. 14).

13.2.4. ***A two-phase star-formation: origin of galactic disks and spheroids***

The above scheme, best-fitting the available IR data as discussed in Sect. 11, implies that *star formation in galaxies has proceeded in two phases: a quiescent one taking place during most of the Hubble time, slowly building stars with standard IMF from the regular flow of gas in rotational supported disks; and a transient actively starbursting phase, recurrently triggered by galaxy mergers and interactions.* During the merger, *violent relaxation* redistributes old stars, producing de Vaucouleur profiles typical of galaxy spheroids, while young stars are generated following a top-heavy IMF.

Because of the geometric (thin disk) configuration of the diffuse ISM and the modest incidence of dusty molecular clouds, the quiescent phase is only moderately affected by dust extinction, and naturally originates most of the optical/NIR background (included early-type galaxies completely deprived of an ISM).

The merger-triggered active starburst phase is instead characterized by a large-scale redistribution of the dusty ISM, with bar-modes and shocks, compressing a large fraction of the gas into the inner galactic regions and triggering formation of molecular clouds. As a consequence, this phase is expected to be heavily extinguished and the bulk of the emission to happen at long wavelengths, naturally originating the cosmic CIRB background. Based on dynamical considerations, we expect that during this violent SB phase the elliptical and S0 galaxies are formed in the most luminous IR SBs at higher-z (corresponding to the SCUBA source population), while galactic bulges in later-type galaxies likely originate in lower IR luminosity, lower-z SBs (the ISO mid-IR population).

The presently available IR data cannot assess if the different luminosity ranks of SCUBA and ISO selected sources are characterized also by different formation timescales (SF activities being confined to the higher-z for the former and to lower-z for the latter), since the present samples are far dominated by K-correction and selection effects. Assumed however this is indeed the case, this could still be reconciled with the expectations of hierarchical clustering models if we consider that SCUBA sources likely trace the very high-density (galaxy clusters) environment with an accelerated merging rate at high-z, while ISO sources are likely related with lower-density environments (galaxy groups or the field) entering the non-linear collapse phase at later cosmic epochs (e.g. Franceschini et al. 1999).

Finally, *if indeed the IMF characteristic of the SB phase is deprived of low-mass stars, as suggested in the previous paragraphs, a consequence would be that the excess blue stars formed during the SB would quickly disappear, leaving the colors of the emerging remnant as typically observed for early-type galaxies and keeping consistent with the evidence that the stellar mass content in galaxies does not change much for* $z < 1$.

13.3. Contribution by gravitational accretion to the global energetics

The remarkable similarities between the cosmic evolution of galaxy and AGN emissivities have been taken as evidence that the same processes triggering SF also make a fraction of the gas to accrete and fuel the AGN (Hasinger Franceschini et al. 1999). Furthermore, detailed studies of local high-luminosity IR galaxies are showing that SF and AGN activities happen very often concomitantly in the same object (Genzel et al. 1998; Risaliti et al. 2000; Bassani et al. 2000). After all, this is a natural outcome of the scheme discussed in previous Sections, the violent radial inflow of gas following the merger/interaction should likely fuel not only nuclear star-clusters, but the BH itself at some stage.

Waiting for forthcoming and future powerful instrumentation (X-ray observatories CHANDRA and XMM, Constellation-X and XEUS in the future, and large space IR observatories like NGST and FIRST) to have a detailed quantification of the relative merits of the two fundamental baryon drivers, some order-of-magnitude estimates may be useful as a guideline. From a combined analysis of the AGN and starburst average bolometric emissivities as a function of redshift, Franceschini et al. (1999) infer a relationship between the mass $M_{\rm BH}$ of the local remnant super-massive BH after the AGN phase to the mass M_* in galactic stars from the SB phase:

$$M_{BH} \simeq 0.001 \left(\frac{\epsilon}{0.001}\right) \left(\frac{0.1}{\eta}\right) \left(\frac{n[type\ II]/n[type\ I]}{5}\right) M_*, \quad (13.35)$$

where η is the radiative efficiency by BH accretion and n[*type II*] / n[*type I*] is the ratio of the absorbed to unabsorbed AGNs (which should be close to 3-5 to explain the local AGN statistics and the observed intensity of the XRB). On the other hand, observations of supermassive BH's in local spheroidal galaxies (Magorrian et al. 1998, Faber et al. 1997) indicate a quite higher mass in the BH accreted material with respect to that in stars: $M_{\rm BH} \simeq$ (0.002 - 0.006) M_*. Assumed that η should not be lower than 0.1, this may require a stellar mass-energy conversion efficiency $\epsilon >>$ 0.001, which is further independent support to the idea of a top-heavy IMF during the SB phase.

14. CONCLUSIONS

During the last few years a variety of observational campaigns, in particular by ISO from space in the far-IR and by large mm telescopes from ground, have started to provide a complementary view of the distant universe at long wavelengths with respect to that offered by standard optical-UV-NIR deep explorations. Also of crucial importance in this context was the discovery of an intense diffuse background radiation in the far-IR/sub-mm of extragalactic origin, the CIRB. These results are challenging those obtained from optical-UV observations only, by revealing luminous to very luminous phases in galaxy evolution at substantial redshifts, likely corresponding to violent events of star-formation in massive systems. In the most extreme of these sources, however, a quasar contribution cannot be excluded, and sometimes has indeed been proven.

Whereas the process of optical identification and spectroscopic characterization of the long-wavelength selected high-redshift sources is only at the beginning (and will keep being a challenging task for the next several years because of the faintness of the optical counterparts), some interesting constraints on the cosmic evolution can already been inferred from observations of the CIRB spectral intensity and the multi-wavelength source counts. The most robust conclusions at the moment appear to be those of a very rapid increase of galaxy long-wavelength emissivity with redshift, paralleled by an increased incidence in high-redshift sources of dust extinction and thermal dust reprocessing with respect to locally observed sources.

A way to interprete these results is to consider as a crucial cosmogonic ingredient the role of galaxy interactions and merging. The strong increases with redshift of the *probability* of interactions (as partly due to a plain geometrical effect in the expanding universe) and of the *effects* of interactions (due to the more abundant fuel avaliable in the past), likely explain the observed rapid evolution.

Altogether, the large energy content of the CIRB is not easily explained, unless the powerful infrared starburst phase is characterized by a stellar IMF somewhat deprived in low-mass stars.

Although the subject is presently subject to some controversies, we think we have provided enough evidence, based on

pioneering efforts of deep sky surveys in the IR and mm, that only such long wavelengths contain the clue to an exhaustive description of the star formation phenomenon, now and in the past. It seems clear that there are no alternatives, neither in X-rays, optical nor radio, to the IR/mm flux measurement for a reliable determinantion of the rate of SF in galaxies, simply because it is there that a dominant fraction of photons from young very luminous stars emerges, and no ways are available to determine "a priory" what precisely this fraction is. Fundamental aspects of galaxy formation and evolution (e.g. the origin of galaxy spheroids, and the onset of quasar activity) can effectively be observed at long wavelengths. In this sense the variety of ground-based and space projects in this field planned for the present decade promises extremely rewarding benefits for observational cosmology.

This paper has benefited by a large collaboration, in particular concerning items discussed in the last chapters, including some yet unpublished results. I want to mention the people who have particularly contributed: H. Aussel, S. Bressan, C. Cesarsky, D. Clements, FX. Desert, D. Elbaz, D. Fadda, R. Genzel, G.L. Granato, M. Harwit, S. Oliver, B. Poggianti, J.L. Puget, D. Rigopoulou, M. Rowan-Robinson, L. Silva. I am also glad to thank L. Danese, G. De Zotti for a long-standing collaboration in this field, A. Cavaliere and C. Chiosi for many fruitful discussions. Finally, I want to warmly thank the organizers of the Canary Islands Winter School on "High-Redshift Galaxies" for their kind invitation.

REFERENCES

1. Adelberger, K. L., Steidel, C. C., 2000, ApJ in press (astro-ph/0001126).
2. Altieri, B., Metcalfe, L., Kneib, J.P., et al., 1999, A&A 343, L65
3. Andreani, P., Franceschini, A., 1996, MNRAS 283, 85.
4. Auriemma, C., Perola, G. C., Ekers, R. D., Fanti, R., Lari, C., Jaffe, W. J., Ulrich, M. H., 1977, A&A 57, 41.
5. Aussel, H., 1999, PhD thesis, CEA Saclay, Paris.
6. Aussel H., Cesarsky C., Elbaz D., Starck, J.L. 1999, A&A 342, 313.
7. Aussel, H., et al., 2000, in preparation.
8. Barger, A. J., Cowie, L. L., Sanders, D. B., Fulton, E., Taniguchi, Y., Sato, Y., Kawara, K., Okuda, H., 1998, Nature 394, 248.
9. Barger, A. J., Cowie, L. L., Smail, I., Ivison, R. J., Blain, A. W., Kneib, J.-P, 1999, AJ 117, 2656.
10. Barger, A., Cowie, L., Mushotzky, R., Richards, E., 2000, ApJ submitted (astro-ph/0007175).
11. Barnes, J.E., & Hernquist, L.E., 1992, ARAA 30, 705.
12. Barnes, J.E., Hernquist, L., 1996, ApJ 471, 115.
13. Bassani, L., Franceschini, A., Malaguti, G., Cappi, M., Della Ceca, R., 2000, A&A submitted.
14. Bertin, E., Dennefeld, M., Moshir, M., 1997, A&A 323, 685.
15. Bertoldi, F., et al., 2000, A&A in press (astro-ph/0006094).
16. Bohren, C.F., Huffman, D.R., 1983, "Absorption and scattering of light by small particles", John Wiley, New York.
17. Boulanger, F., Boisssel, P., Cesarsky, D. Ryter, C., 1998, A&A 339, 194.
18. Bruzual, A.G., 1983, ApJ 273, 105.
19. Calzetti, D., 1997, AJ 113, 162.
20. Cappi, M., et al., 1999, A&A 350, 777.
21. Carilli, C.L., Yun, M.S., 1999, ApJ Letters 513, L13.
22. Cavaliere, A., & Vittorini, V., 2000, ApJ in press (astro-ph/0006194).
23. Chapman, S.C., 2000, MNRAS in press (astro-ph/9909092).
24. Chini, R., Krugel, E., Lemke, D., Ward-Thompson, D., 1995, A&A 295, 317.
25. Clements, D., Baker, A., 1997, in "Extragalactic Astronomy in the Infrared", Edited by G. A. Mamon, Trinh Xuan Thuan, and J. Tran Thanh Van. Paris, Editions Frontieres, p. 347
26. Cohen, J., et al., 1999, in press (astro-ph/9912048).
27. Condon, J.J., 1974, ApJ 188, 279.
28. Condon, J. J., 1992, ARAA 30, 575.
29. Coppi, P., Aharonian, F., 1999, Astropart. Phys. 11, 35-39
30. de Jong, T., Klein, U., Wielebinski, R., Wunderlich, E., 1985, A& A Letters 147, L6.
31. De Zotti, G., Franceschini, A., Toffolatti, L., Mazzei, P., Danese, L., 1996, Astro. Lett. and Communications 35, 289.
32. Desert F.X., et al., 1999, A&A 342, 363.
33. Devriendt, J. E. G., Guiderdoni, B., Sadat, R., 1999, A&A 350, 381.
34. Disney, M., Davies, J., Phillipps, S., 1989, MNRAS 239, 939.
35. Dole, H., Gispert, R., Lagache, G., et al., 2000, in *ISO Beyond Point Sources, Studies of Extended Infrared Emission*, R. Laureijs, K. Leech and M. Kessler Eds., ESA-SP 455, 167.
36. Downes, D., et al., 1999, A&A 347, 809.
37. Draine, B. T., & Lee, H. M. 1984, ApJ 285, 89.
38. Dunne, L., Eales, S. Edmunds, M., Ivison, R., Alexander, P., Clements, D., 2000, MNRAS 315, 115.
39. Dwek, E., 1998, ApJ 501, 643.
40. Dwek, E., Arendt, R. G., 1998, ApJ Letters 508, L9.

41. Eales, S., et al., 1999, ApJ 515, 518.
42. Elbaz D., et al., 1999, A&A Letters 351, L37.
43. Elbaz D., 1999, Proceedings of Rencontres de Moriond, "Building Galaxies, from the Primordial Universe to the Present", F. Hammer, et al. Eds, (Ed. Frontieres, astro-ph/9911050).
44. Ellis, R. S., 1997, ARAA 35, 389.
45. Ellis, R. S., Colless, M., Broadhurst, T., Heyl, J., Glazebrook, K., 1996, MNRAS 280, 235.
46. Faber, S.M., et al., 1997, AJ 114, 1771.
47. Fabian, A., et al., 2000, MNRAS 315, 8.
48. Fang F., Shupe, D.L., Xu, C., Hacking, P.B. 1998, ApJ 500, 693.
49. Finkbeiner, D.P., Davies, M., Schlegel, D.J., 2000, ApJ in press (astro-ph/0004175).
50. Fixsen D.J., et al. 1998, ApJ 508, 123.
51. Flores H., Hammer F., Thuan T. et al. 1999, ApJ 517, 148.
52. Franceschini, A., Danese, L., de Zotti, G., Xu, C., 1988, MNRAS 233, 175.
53. Franceschini, A., Mazzei, P., De Zotti, G., Danese, L., 1994, ApJ 427, 140.
54. Franceschini, A., La Franca, F., Cristiani, S., Martin-Mirones J., 1994b, MNRAS 269, 683.
55. Franceschini, A., Andreani, P., Danese, L., 1998, MNRAS 296, 709.
56. Franceschini, A., Hasinger, G., Miyaji, T., Malquori, D., 1999, MNRAS 310, L5.
57. Franceschini, A., Aussel, H., Elbaz, D., et al., 2000, Mem Sait, in press.
58. Franceschini, A., et al., 2000, in preparation.
59. Frayer, D.T., et al., 1999, ApJ Letters 514, 13L.
60. Genzel, R., & Cesarsky, C.J., 2000, ARAA in press (astro-ph/0002184).
61. Genzel, R., et al., 1998, ApJ 498, 579.
62. Gibson, B. K., Loewenstein, M., Mushotzky, R. F., 1997, MNRAS 290, 623.
63. Gispert, R., Lagache, G., Puget, J. L., 2000, AA in press (astro-ph/0005554).
64. Gordon, K.D., Calzetti, D., Witt, A.N., 1997, ApJ 487, 625.
65. Gorjian, V., Wright, E. L., Chary, R. R., 2000, ApJ 536, 550.
66. Granato, G.L., Danese, L., 1994, MNRAS 268, 235.
67. Granato, G.L., Danese, L., Franceschini, A., 1997, ApJ 486, 147.
68. Granato, G.L., et al., 2000, MNRAS in press (astro-ph/0001308).
69. Gregorich, D. T., Neugebauer, G., Soifer, B. T., Gunn, J. E., Herter, T. L., 1995, AJ 110, 259.
70. Guhathacurta, P., Draine, B.T., 1989, ApJ 346, 230.
71. Guiderdoni, B., et al., 1997, Nature 390, 257.
72. Haarsma, D. B., Partridge, R. B., 1998, ApJ Letters 503, L5.
73. Hacking, P., Houck, J. R., 1987, ApJS 63, 311.
74. Hacking, P., Houck, J. R., Condon, J. J., 1987, ApJ Letters 316, L15.
75. Harwit, M., 1999, ApJ Letters 510, L83.
76. Harwit, M., Pacini, F., 1975, ApJ Letters 200, L127.
77. Harwit, M., Protheroe, R. J., Biermann, P. L., 1999, ApJ Letters 524, 91.
78. Hasinger, G., 1998, Astronomische Nachrichten 319, 37.
79. Hauser, M.G., Arendt, R.G., Kelsall, T., et al. 1998, ApJ 508, 25.
80. Heckman, T.M., Armus, L., Miley, G., 1990, ApJS 74, 833.
81. Helou, G., Soifer, B. T., Rowan-Robinson, M., 1985, ApJ Letters 298, L7.
82. Hornschemeier, A.E., Brandt, W.N., Garmire, G.P., 2000, ApJ in press (astro-ph/0004260).
83. Hoyle, F., Wickramasinghe, N.C., 1991, *The theory of cosmic grains*, Kluwer Academic Publishers.
84. Hughes, D., et al., 1998, Nature 394, 241.
85. Iuvela, M., Mattila, K., & Lemke, D., 2000, A& A in press (astro-ph/0005510).
86. Ivison, R.J., Dunlop, J.S., Smail, I., Dey, A., Liu, M., Graham, J., 2000, ApJ in press (astro-ph/0005234).
87. Jimenez, R., Padoan, P., Dunlop, J., Bowen, D., Juvela, M., Matteucci, F., 2000, ApJ 532, 152.
88. Kennicut, R.C., 1998, ARAA 36, 189.
89. Kormendy, J., Sanders, D., 1992, ApJ Letters 390, 53.
90. Krawczynski, H., Coppi, P.S., Maccarone, T., Aharonian, F.A., 2000, A&A 353, 97.
91. Lagache, G., Puget, J. L., 2000, A&A 355, 17L.
92. Lagache G., Abergel, A., Boulanger, F., Desert, F.X., Puget J.L., 1999, A&A 344, 322L.
93. Lagage, P.O., et al., 1996, A&A 315, L273.
94. Lari, C., et al., 2000, A&A submitted.
95. Le Fevre, O., et al., 2000, MNRAS 311, 565.
96. Lehnert, M., Heckman, T.M., 1996, ApJ 462, 651.
97. Leitherer, C., Heckman, T.M., 1995, ApJS 96, 9.
98. Leitherer, C., et al., 1999, ApJS 123, 3.
99. Lilly, S.J., et al., 1999, ApJ 518, 641.
100. Lonsdale, Carol J., Hacking, Perry B., Conrow, T. P., Rowan-Robinson, M., 1990, ApJ 358, 60.

101. Lutz, D., Spoon, H. W. W., Rigopoulou, D., Moorwood, A. F. M., Genzel, R., 1998, ApJ Letters 505, L103.
102. Madau, P., Pozzetti, L., 2000, MNRAS Letters 312, 9.
103. Madau, P., et al., 1996, MNRAS 283, 1388.
104. Magorrian, J., et al., 1998, AJ 115, 2285.
105. Matsuhara, H., et al., 2000, A& A in press (astro-ph/0006444).
106. Mazzei, P., de Zotti, G., Xu, C., 1994, ApJ 422, 81.
107. Mazzei, P., Aussel, H., Xu, C., Salvo, M., de Zotti, G., Franceschini, A., 2000, A& A submitted
108. Meurer, G. R., Heckman, T. M., Lehnert, M. D., Leitherer, C., Lowenthal, J., 1997, AJ 114, 54.
109. Mie, G., 1908, Ann. Physik 25, 377.
110. Miyaji, T., Hasinger, G., Schmidt., M., 2000, A&A 353, 25.
111. Moorwood, A., 1996, Space Science Reviews 77, 303.
112. Moorwood, A., Origlia, L., Kotilainen, J., Oliva, E., 1996, in Proceedings of the ESO Symposium on Spiral Galaxies, Springer-Verlag, Berlin, 299.
113. Mushotzky, R. F., Loewenstein, M., 1997, ApJ Letters 481, 63.
114. Norman, C.A., Scoville, N.Z., 1988, ApJ 332, 124.
115. Oliver, S., et al., 1996, MNRAS 280, 673.
116. Oliver, S., et al., 2000a, MNRAS in press (astro-ph/0003263).
117. Oliver, S., et al., 2000b, MNRAS submitted.
118. Padoan, P., Juvela, M., Bally, J., Nordlund, A., 1998, ApJ 504, 300.
119. Pearson, C., Rowan-Robinson, M., 1996, MNRAS 283, 174.
120. Pier, E.A., Krolik, J.H., 1992, ApJ 401, 99.
121. Poggianti, B.M., Bressan, A., & Franceschini, A., 2001, ApJ 550, 195.
122. Poggianti, B.M., Wu, H., 2000, ApJ 529, 157.
123. Puget, J.L., Leger, A., 1989, ARAA 27, 161.
124. Puget, J. L., Léger, A., & Boulanger, F. 1985, A&A 142, L19.
125. Puget J.-L., et al. 1996, A&A 308, L5.
126. Puget, G.L., Lagache, G., Clements, D., Reach W., Aussel, H., Bouchet, F., Cesarsky, C., Desert, F., Dole, H., Elbaz, D., Franceschini, A., Guiderdoni, B., Moorwood, A., 1999, A&A 345, 29.
127. Rieke, G. H., Lebofsky, M. J., Thompson, R. I., Low, F. J., Tokunaga, A., 1980, ApJ 238, 24.
128. Rieke, G. H., Lebofsky, M. J., Walker, C. E., 1988, ApJ 325, 679.
129. Rigopoulou, D., Franceschini, A., Aussel, H., et al., 2000, ApJ Letters, 537, L85.
130. Risaliti, G., Gilli, R., Maiolino, R., Salvati, M., 2000, A&A 357, 13
131. Rowan-Robinson, M., Saunders, W., Lawrence, A., Leech, K., 1991, MNRAS 253, 485.
132. Rowan-Robinson, M. 1992, MNRAS 258, 787.
133. Rowan-Robinson, M., et al., 1997, MNRAS 289, 490.
134. Rush, B., Malkan, M.A., Spinoglio, L., 1993, ApJS 89, 1.
135. Rybicki, G.B., Lightman, A.P., 1979, "Radiative Processes in Astrophysics", J. Wiley & Sons.
136. Sanders, D., et al., 1988, ApJ 325, 74.
137. Sanders, D., & Mirabel, I.F., 1996, ARAA 34, 749.
138. Saunders, W., Rowan-Robinson, M., Lawrence, A., Efstathiou, G., Kaiser, N., Ellis, R. S., Frenk, C. S., 1990, MNRAS 242, 318.
139. Saunders, W., et al., 1997, in *Extragalactic Astronomy in the Infrared*, G. A. Mamon, Trinh Xuan Thuan, and J. Tran Thanh Van. Eds, Paris, Editions Frontieres, 431.
140. Scheuer, P.A.G., 1957, Proc. Cambridge Phil. Soc. 53, 764.
141. Scott, D., et al., 2000, A&A Letters 357, L5.
142. Scoville, N.Z., Yun, M.S., Bryant, P.M., 1996, in *Cold gas at high redshifts*, M. Bremer et al. Eds., Kluwer Academic Publishers, 25.
143. Siebenmorgen, R., Krugel, E., 1992, A&A 259, 614.
144. Siebenmorgen, R., Rowan-Robinson, M., Efstathiou, A., 2000, MNRAS 313, 734.
145. Silva, L., Granato, G.L., Bressan, A., Danese, L., 1998, ApJ 509, 103.
146. Smail, I., Ivison, R. J., Blain, A. W., 1997, ApJ Letters 490, L5.
147. Smail, I., et al., 1999, MNRAS 308, 1061.
148. Soifer, B. T., Neugebauer, G., Matthews, K., et al., 2000, AJ 119, 509.
149. Spinoglio, L., Malkan, M. A., 1992, ApJ 399, 504.
150. Stanev, T., Franceschini, A., 1998, ApJ Letters 494, L159.
151. Starck, J. L., Aussel, H., Elbaz, D., Fadda, D., Cesarsky, C., 1999, A& AS 138, 365.
152. Stecker, F., De Jager, O., Salamon, M., 1992, ApJL 390, L49.
153. Taniguchi, Y., Cowie, L.L., Sato, Y., Sanders, D., Kawara, K., 1997, A&A 328, L9
154. Telesco, C., 1988, ARAA 26, 343.
155. Tinsley, B.M., 1977, ApJ 211, 621.
156. Toffolatti, Franceschini A., De Zotti G., Danese L., 1987, A&A 184, 7.

157. Toomre, A., 1977, in *The evolution of galaxies and their stellar populations*, Yale University Observatory, 401.
158. van der Werf, P., 1996, in *Cold Gas at High Redshift*, M. Bremer et al. Eds, Kluwer Academic Publishers, 37.
159. Vigroux, L., et al., 1998, in *The Universe as seen by ISO*, ESA-SP 427, 805.
160. Xu, C., 1997, in *Extragalactic Astronomy in the Infrared*, G. A. Mamon, Trinh Xuan Thuan, and J. Tran Thanh Van Eds., Editions Frontieres, Paris, 193.
161. Xu, C., Hacking, P., Fang, F., et al., 1998, ApJ 508, 576.
162. Xu, C., 2000, ApJ in press (astro-ph/0004216).
163. Zoccali, M., et al., 2000, ApJ 530, 418.